Article

cDC1 prime and are licensed by CD4+ T cells to induce anti-tumour immunity

https://doi.org/10.1038/s41586-020-2611-3

Received: 3 December 2019

Accepted: 23 June 2020

Published online: 12 August 2020

Check for updates

Stephen T. Ferris[1,11], Vivek Durai[1,10,11], Renee Wu[1,11], Derek J. Theisen[1], Jeffrey P. Ward[1,2], Michael D. Bern[3], Jesse T. Davidson IV[1,4], Prachi Bagadia[1], Tiantian Liu[1], Carlos G. Briseño[1], Lijin Li[4], William E. Gillanders[4,5], Gregory F. Wu[1,6], Wayne M. Yokoyama[3], Theresa L. Murphy[1], Robert D. Schreiber[1,7,8] & Kenneth M. Murphy[1,9] ✉

Conventional type 1 dendritic cells (cDC1)[1] are thought to perform antigen cross-presentation, which is required to prime CD8+ T cells[2,3], whereas cDC2 are specialized for priming CD4+ T cells[4,5]. CD4+ T cells are also considered to help CD8+ T cell responses through a variety of mechanisms[6–11], including a process whereby CD4+ T cells 'license' cDC1 for CD8+ T cell priming[12]. However, this model has not been directly tested in vivo or in the setting of help-dependent tumour rejection. Here we generated an *Xcr1*^{Cre} mouse strain to evaluate the cellular interactions that mediate tumour rejection in a model requiring CD4+ and CD8+ T cells. As expected, tumour rejection required cDC1 and CD8+ T cell priming required the expression of major histocompatibility class I molecules by cDC1. Unexpectedly, early priming of CD4+ T cells against tumour-derived antigens also required cDC1, and this was not simply because they transport antigens to lymph nodes for processing by cDC2, as selective deletion of major histocompatibility class II molecules in cDC1 also prevented early CD4+ T cell priming. Furthermore, deletion of either major histocompatibility class II or CD40 in cDC1 impaired tumour rejection, consistent with a role for cognate CD4+ T cell interactions and CD40 signalling in cDC1 licensing. Finally, CD40 signalling in cDC1 was critical not only for CD8+ T cell priming, but also for initial CD4+ T cell activation. Thus, in the setting of tumour-derived antigens, cDC1 function as an autonomous platform capable of antigen processing and priming for both CD4+ and CD8+ T cells and of the direct orchestration of their cross-talk that is required for optimal anti-tumour immunity.

CD4+ T cell help for CD8+ T cell responses has been proposed to be mediated by CD40-dependent licensing of antigen-presenting cells[7,8,13]. cDC1 have been suggested as the target of CD4+ T cell help on the basis of in vitro analysis[14] and intravital imaging during viral infection[15,16]. Other mechanisms to explain CD4+ T cell help include the production of interleukin 2[11], prevention of TRAIL expression by CD8+ T cells[10] and direct activation of CD40 signalling in CD8+ T cells[9]. But despite extensive analysis, a requirement for cDC1 in mediating CD4+ T cell help in vivo has not been directly established.

Previous studies suggested that CD4+ T cells are primed predominantly by cDC2, given their superior major histocompatibility class II antigen presentation of soluble ovalbumin or ovalbumin coupled to antibodies targeted to Fc or other surface receptors[4,17]. In support of this possibility, *Irf4*$^{-/-}$ mice, which have impaired cDC2 migration[18], show reduced CD4+ T responses in the intestine and lung to allergens or fungal infections[19,20]. For cell-associated antigens, however, some studies[21,22] report lower major histocompatibility class II processing by cDC2 than by cDC1. A recent study in a tumour model showed that cDC2 induce the proliferation of CD4+ T cells at an advanced stage of tumour growth, but the authors did not examine the ability of these CD4+ T cells to provide help for CD8+ T cell responses[5]. In summary, it is not known whether cDC1 or cDC2 are responsible for priming CD4+ T cells that help anti-tumour CD8+ T cell responses.

CD4+ T cells support anti-tumour responses

CD4+ T cells are required for generating and maintaining CD8+ T cell memory in response to pathogens[23,24]. To determine their role in anti-tumour immunity, we used a methylcholanthrene-induced progressor fibrosarcoma cell line (1956) that, although not initially rejected,

[1]Department of Pathology and Immunology, Washington University School of Medicine, St Louis, MO, USA. [2]Division of Oncology, Department of Medicine, Washington University School of Medicine, St Louis, MO, USA. [3]Division of Rheumatology, Washington University School of Medicine, St Louis, MO, USA. [4]Department of Surgery, Washington University School of Medicine, St Louis, MO, USA. [5]The Alvin J. Siteman Cancer Center at Barnes–Jewish Hospital and Washington University School of Medicine, St Louis, MO, USA. [6]Department of Neurology, Washington University School of Medicine, St Louis, MO, USA. [7]The Andrew M. and Jane M. Bursky Center for Human Immunology and Immunotherapy Programs, Washington University School of Medicine, St Louis, MO, USA. [8]Parker Institute for Cancer Immunotherapy, San Francisco, CA, USA. [9]Howard Hughes Medical Institute, Washington University School of Medicine, St Louis, MO, USA. [10]Present address: Department of Medicine, University of California, San Francisco, San Francisco, CA, USA. [11]These authors contributed equally: Stephen T. Ferris, Vivek Durai, Renee Wu. ✉e-mail: kmurphy@wustl.edu

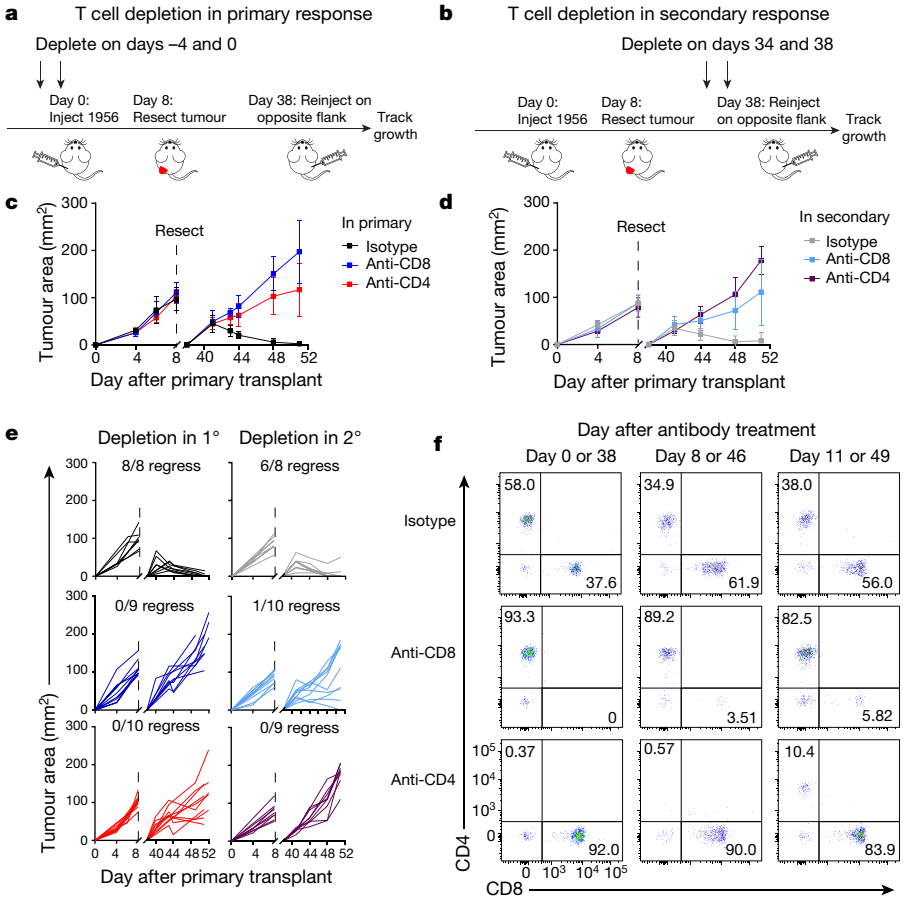

Fig. 1 | CD4⁺ T cells are required during primary and secondary tumour responses. a, **b**, Schematics of the depletion of T cells during primary (**a**) and secondary (**b**) tumour responses. **c**, **d**, Tumour growth curves of mice depleted of CD4⁺ or CD8⁺ T cells during the primary (**c**) and secondary (**d**) implantation of 1956 tumours. Data in each panel represent mean ± s.d. of pooled biologically independent samples from two independent experiments (**c**: $n = 8$ isotype, 9 anti-CD8, 10 anti-CD4; **d**: $n = 8$ isotype, 10 anti-CD8, 9 anti-CD4). **e**, Individual tumour growth curves from mice depleted of CD4⁺ or CD8⁺ T cells after the primary (left) or secondary (right) 1956 tumour implantation. Regress, tumour regression. **f**, T cell populations in peripheral blood after CD4⁺ or CD8⁺ depletion.

induces immunological memory upon implantation into wild-type mice[25]. Here we implanted tumours for eight days (primary challenge) to induce memory and then surgically resected them (Fig. 1a, b). T cell memory was indicated by the subsequent rejection of tumours implanted on the contralateral flank (secondary challenge). Depletion of CD8⁺ T cells during either the primary or the secondary challenge prevented tumour rejection (Fig. 1c–e), consistent with formation of CD8⁺ T cell memory[25]. Moreover, depletion of CD4⁺ T cells during either the primary or the secondary challenge also prevented tumour rejection during the secondary challenge (Fig. 1c–e). CD4⁺ T cells were required early in the tumour immune response, as CD4⁺ T cells returned approximately one week after depletion (Fig. 1f). Unlike results from a similar challenge strategy involving infection with *Listeria monocytogenes*, in which CD4⁺ T cell help was not required for CD8⁺ T cell recall responses[23], our data are in agreement with the recent finding that major histocompatibility class II tumour epitopes at the tumour site may be required to augment tumour rejection dependent on CD8⁺ T cells[26,27].

Early priming of CD4⁺ T cells depends on cDC1

The role of cDC1 in priming CD4⁺ T cells is unclear: some studies show inherently less efficient major histocompatibility class II antigen presentation by cDC1 compared with cDC2[4,5,17], whereas others suggest that cDC1 are important in CD4⁺ T cell priming[21,28]. To evaluate CD4⁺ T cell priming in the setting of tumour rejection, we examined T cell responses to modified 1956 fibrosarcoma cells that express membrane-associated ovalbumin (1956-mOVA)[29] or an empty vector control (1956-EV) (Extended Data Fig. 1a). The expression of 1956-mOVA converted the 1956 cell tumour into a regressor tumour that was cleared by wild-type mice (Extended Data Fig. 1b). This rejection was dependent on CD8⁺ T cells, as *Irf8* +32$^{-/-}$ mice, which lack a cDC1-dependent *Irf8* enhancer and subsequently lack cDC1[30], did not reject the 1956-mOVA tumours (Extended Data Fig. 1c). Furthermore, OVA-specific SIINFEKL-H-2K^{b} tetramer⁺ CD8⁺ T cells expanded in wild-type mice in response to 1956-mOVA, but were absent in mice lacking cDC1, showing that cDC1 prime CD8⁺ T cells (Extended Data Fig. 1d). We next examined early CD4⁺ T cell proliferation in response to 1956-mOVA (Fig. 2a, b) by transferring OT-II transgenic CD4⁺ T cells, the activation of which is specifically induced by major histocompatibility II presentation of ovalbumin, into tumour-bearing mice. OT-II cells underwent cell division in tumour-draining lymph nodes in wild-type mice, consistent with recognition of ovalbumin$_{323–339}$ peptide–major histocompatibility II complexes on some antigen-presenting cells. By contrast, *Irf8* +32$^{-/-}$ mice lacking cDC1 showed markedly lower proliferation of OT-II cells (Fig. 2a, b). In summary, in the 1956-mOVA tumour model, cDC1 act as the primary antigen-presenting cells for early presentation to naive CD4⁺ T cells.

To test this result in another model, we generated a B16F10 melanoma cell line stably expressing membrane-associated ovalbumin

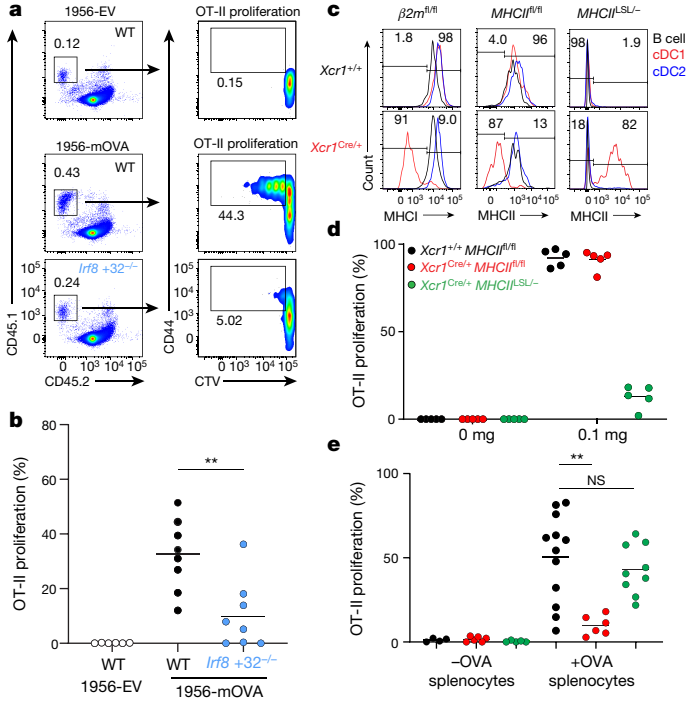

Fig. 2 | cDC1 are superior at presenting cell-associated material. **a**, Representative flow plots of percentages of proliferated OT-II cells transferred into wild-type (WT) B6 and *Irf8* +32$^{-/-}$ mice injected with 10^6 1956-EV or 1956-mOVA. CTV, Cell Trace Violet. **b**, Graph of data in **a**. Data are pooled biologically independent samples from three independent experiments ($n = 6$ for wild-type 1956-EV, 8 for all other groups). $^{**}P = 0.007$. **c**, *Xcr1*$^{+/+}$ (top) and *Xcr1*$^{Cre/+}$ (bottom) splenic antigen-presenting cells stained for major histocompatibility class I and II expression from *β2m*$^{fl/fl}$ (left), *MHCII*$^{fl/fl}$ (middle) and *MHCII*$^{LSL/-}$ mice (right). **d**, **e**, Percentages of proliferated OT-II transferred into *Xcr1*$^{+/+}$ *MHCII*$^{fl/fl}$, *Xcr1*$^{Cre/+}$ *MHCII*$^{fl/fl}$ and *Xcr1*$^{Cre/+}$ *MHCII*$^{LSL/-}$ mice immunized with soluble ovalbumin (**d**) or cell-associated ovalbumin (**e**) on day 0. Data are pooled biologically independent samples from two independent experiments, $n = 5$ for all groups (**d**), or four independent experiments, $n = 4$ for *Xcr1*$^{+/+}$ *MHCII*$^{fl/fl}$ without ovalbumin (−OVA), 6 for *Xcr1*$^{Cre/+}$ *MHCII*$^{fl/fl}$ −OVA, 5 for *Xcr1*$^{Cre/+}$ *MHCII*$^{LSL/-}$ −OVA, 12 for *Xcr1*$^{+/+}$ *MHCII*$^{fl/fl}$ +OVA, 6 for *Xcr1*$^{Cre/+}$ *MHCII*$^{fl/fl}$ +OVA, 9 for *Xcr1*$^{Cre/+}$ *MHCII*$^{LSL/-}$ +OVA (**e**). $^{**}P = 0.002$; NS, not significant. **b**, **e**: unpaired, two-tailed Mann–Whitney test.

(B16F10-mOVA) and, as a control, B16F10 cells expressing only the empty retroviral vector (B16F10-EV) (Extended Data Fig. 2a). We examined in vivo CD4$^+$ T cell proliferation in response to B16F10-mOVA following adoptive transfer of OT-II T cells into tumour-bearing mice from both groups (Extended Data Fig. 2b). Early OT-II proliferation was robust in the wild-type mice, but markedly less so in the *Irf8* +32$^{-/-}$ mice lacking cDC1, similar to the results obtained using 1956-mOVA tumours (Fig. 2a, b). This implies that cDC1 may generally function as antigen-presenting cells for CD4$^+$ T cells in response to cell-associated tumour antigens.

Our finding that cDC1 are required for CD4$^+$ T cell priming could result from a possible role in transporting antigens to draining lymph nodes, where antigens could be transferred to cDC2 for presentation to CD4$^+$ T cells. In this case, major histocompatibility class II expression by cDC1 should be dispensable for CD4$^+$ T cell priming. To test this, we generated an *Xcr1*^{Cre} mouse strain to allow the conditional inactivation of major histocompatibility class II expression specifically in cDC1 (Extended Data Fig. 3a–c). In mice with one *Xcr1*^{Cre} allele (*Xcr1*$^{Cre/+}$), mCherry and Cre recombinase activity, as reported by *Rosa26*–lox-stop-lox–eYFP (R26^{LSLYFP})[31] in which Cre expression removes the stop codon, allowing *Rosa26*-driven expression of eYFP in a cell-type-specific manner, were detected specifically in cDC1, but not in cDC2 or other immune lineages (Extended Data Fig. 3d–j). *Xcr1*^{Cre} mice efficiently deleted major histocompatibility class I or II surface expression from cDC1, but not other lineages, when crossed with mice carrying alleles of β2 microglobulin flanked by *loxP* sites (floxed; *B2m*$^{fl/fl}$, or *β2m*$^{fl/fl}$)[32] or floxed alleles of *H2-Ab1* (*MHCII*$^{fl/fl}$)[33], respectively (Fig. 2c, Extended Data Figs. 4–6). Furthermore, by crossing *Xcr1*^{Cre} mice with mice carrying a conditional knockout of *H2-Ab1* containing a floxed stop sequence (*H2-Ab1* stop$^{fl/fl}$, or IA$_\beta{}^b$stop$^{f/f}$; *MHCII*^{LSL})[34], we achieved major histocompatibility class II expression exclusively in cDC1, but not other lineages (Fig. 2c). In mice lacking either major histocompatibility class I or II molecules specifically on cDC1, cDC1 development was normal (Extended Data Fig. 6a, b).

As a control, we first examined mice lacking major histocompatibility class I expression on cDC1. We transferred ovalbumin-specific OT-I transgenic CD8$^+$ T cells to mice and then immunized them with different forms of antigen. OT-I proliferation was only partially reduced in response to soluble ovalbumin in *Xcr1*$^{Cre/+}$ *β2m*$^{fl/fl}$ compared to *Xcr1*$^{+/+}$ *β2m*$^{fl/fl}$ mice, but was completely absent in *Xcr1*$^{Cre/+}$ *β2m*$^{fl/fl}$ mice in response to cell-associated antigens (Extended Data Figs. 4 and 6c). This is in agreement with our previous report that cDC2 efficiently cross-present soluble, but not cell-associated, antigens in vivo[22].

We next evaluated OT-II proliferation in *Xcr1*$^{Cre/+}$ *MHCII*$^{fl/fl}$ mice (Fig. 2d, e). OT-II cells proliferated in response to soluble ovalbumin equivalently in *Xcr1*$^{Cre/+}$ *MHCII*$^{fl/fl}$ and wild-type (*Xcr1*$^{+/+}$ *MHCII*$^{fl/fl}$) control mice (Fig. 2d, Extended Data Fig. 5c). By contrast, OT-II cell proliferation in response to cell-associated antigen was substantially lower in *Xcr1*$^{Cre/+}$ *MHCII*$^{fl/fl}$ than in wild-type mice (Fig. 2e, Extended Data Fig. 5d). These results suggest that major histocompatibility class II expression on cDC1 is needed for optimal CD4$^+$ T cell priming in response to cell-associated antigens. As a control, we found that OT-I proliferation in response to cell-associated ovalbumin was similar in *Xcr1*$^{Cre/+}$ *MHCII*$^{fl/fl}$ and wild-type mice (Extended Data Fig. 6e). Moreover, *Xcr1*$^{Cre/+}$ *MHCII*$^{LSL/-}$ mice, which express major histocompatibility class II molecules exclusively on cDC1, induced OT-II proliferation in response to cell-associated, but not soluble, ovalbumin (Fig. 2d, e, Extended Data Fig. 6d), suggesting that major histocompatibility class II expression by cDC1 is sufficient for CD4$^+$ responses to cell-associated antigens.

We next asked whether this effect also occurs with tumour-derived antigens (Fig. 3). As a control, we confirmed that *Xcr1*$^{+/+}$ *MHCII*$^{fl/fl}$ (wild-type) mice, which express major histocompatibility class II molecules normally on cDC1, rejected 1956-mOVA tumours, as expected (Fig. 3a). By contrast, *Xcr1*$^{Cre/+}$ *MHCII*$^{fl/fl}$ mice, lacking major histocompatibility class II expression on cDC1, did not reject these tumours (Fig. 3a). *MHCII*$^{LSL/-}$ mice, which lack all major histocompatibility class II expression, including on thymic epithelial cells, and consequently lack mature CD4$^+$ T cells (Extended Data Fig. 5a), also did not reject 1956-mOVA tumours (Fig. 3a), consistent with a requirement for CD4$^+$ T cell help to generate CD8$^+$ T cell responses sufficient for tumour rejection. Moreover, the numbers of T regulatory cells (Tregs) did not differ between *Xcr1*$^{Cre/+}$ *MHCII*$^{fl/fl}$ and control *MHCII*$^{fl/fl}$ mice (Extended Data Fig. 5b), although we were unable to measure the numbers of tumour-specific endogenous Tregs in this system. In summary, rejection of the 1956-mOVA tumour requires expression of major histocompatibility class II by cDC1.

In addition, we found that optimal priming of both CD8$^+$ and CD4$^+$ T cells induced against the 1956-mOVA tumour was regulated by the expression of major histocompatibility class II by cDC1. First, as compared to control mice, *Xcr1*$^{Cre/+}$ *MHCII*$^{fl/fl}$ mice showed significantly weaker expansion of SIINFEKL-H-2K^b tetramer$^+$ endogenous CD8$^+$ T cells in response to 1956-mOVA tumours (Fig. 3b), indicating that a direct interaction between CD4$^+$ T cells and cDC1 regulates the CD8$^+$ T cell response in tumour rejection. Moreover, early priming of CD4$^+$ T cells in vivo during the response to tumour-derived antigens required direct interactions with cDC1, rather than cDC2 (Fig. 3c). We observed robust OT-II proliferation in tumour-draining lymph nodes in wild-type mice implanted with 1956-mOVA, but significantly weaker OT-II proliferation

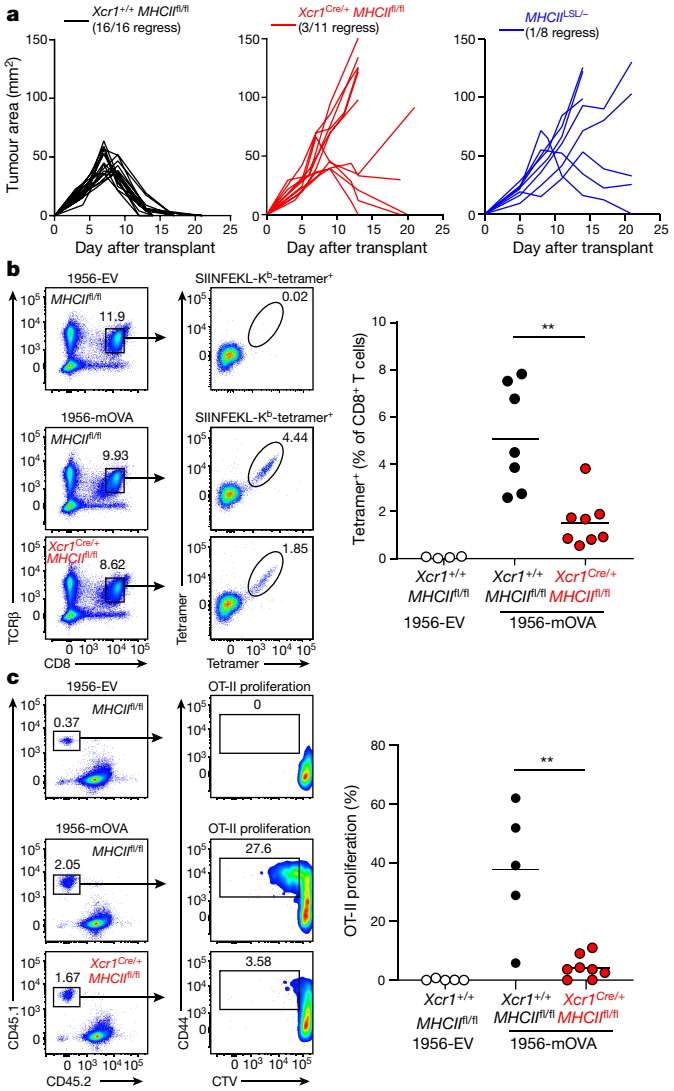

Fig. 3 | cDC1 expression of major histocompatibility class II is required for tumour rejection. a, Tumour growth curves of *Xcr1*$^{+/+}$ *MHCII*$^{fl/fl}$ (left), *Xcr1*$^{Cre/+}$ *MHCII*$^{fl/fl}$ (middle) and *MHCII*$^{LSL/-}$ mice (right) injected with 10^6 1956-mOVA. **b**, Mice of the same three genotypes were injected with 10^6 1956-EV or 1956-mOVA, and spleens were stained for the presence of SIINFEKL-K^b-tetramer$^+$ CD8$^+$ T cells. Left, representative flow plots of percentages of tetramer$^+$ CD8$^+$ T cells. Right, tetramer$^+$ CD8$^+$ T cells as a percentage of all CD8$^+$ T cells. Data are pooled biologically independent samples from two independent experiments ($n = 4$ for *Xcr1*$^{+/+}$ *MHCII*$^{fl/fl}$ 1956-EV, 7 for *Xcr1*$^{+/+}$ *MHCII*$^{fl/fl}$, 8 for *Xcr1*$^{Cre/+}$ *MHCII*$^{fl/fl}$). $^{**}P = 0.001$. **c**, *Xcr1*$^{+/+}$ *MHCII*$^{fl/fl}$ and *Xcr1*$^{Cre/+}$ *MHCII*$^{fl/fl}$ mice were injected with 10^6 1956-EV or 10^6 1956-mOVA. Left, representative flow plots of OT-II T cells three days after transfer. Right, percentages of proliferated OT-II cells transferred. Data are pooled biologically independent samples from two independent experiments ($n = 8$ for *Xcr1*$^{Cre/+}$ *MHCII*$^{fl/fl}$, 5 for all other groups). $^{**}P = 0.006$. **b**, **c**: unpaired, two-tailed Mann–Whitney test.

in *Xcr1*$^{Cre/+}$ *MHCII*$^{fl/fl}$ mice (Fig. 3c). OT-I proliferation in vivo was not reduced, as compared to that in controls, either after transfer into tumour-bearing *Xcr1*$^{Cre/+}$ *MHCII*$^{fl/fl}$ mice or after co-culture ex vivo with cDC1 collected from tumour-draining lymph nodes (Extended Data Fig. 6e–g). This ex vivo result suggests that major histocompatibility class II expression on cDC1 is not required for antigen presentation restricted by major histocompatibility class I expression during the initial tumour immune response, but is required for in vivo expansion or persistence of activated CD8$^+$ T cells. In summary, in the context of cell-associated tumour antigens, early CD4$^+$ T cell priming depends primarily on cDC1, whereas with soluble antigens, priming depends primarily on cDC2.

Optimal T cell priming requires cDC1 CD40 signalling

CD4$^+$ T cell help has been suggested to operate by CD40 signalling on cDC1[35]. To test the requirement for CD40 signalling in cDC1 for tumour rejection, we generated *Xcr1*$^{Cre/+}$ *Cd40*$^{fl/fl}$ mice, in which CD40 is absent on cDC1 but expressed normally on cDC2 and B cells (Extended Data Fig. 7a). Control *Xcr1*$^{+/+}$ *Cd40*$^{fl/fl}$ (wild-type) mice rejected 1956-mOVA, as expected, but *Xcr1*$^{Cre/+}$ *Cd40*$^{fl/fl}$ mice did not (Fig. 4a). This failure was not due to defects in cDC1 development, as *Xcr1*$^{Cre/+}$ *Cd40*$^{fl/fl}$ mice had normal cDC1 numbers with a normal transcriptional signature (Fig. 4b, Extended Data Fig. 7b). In particular, cDC1 isolated from either the spleen or the lymph nodes of *Xcr1*$^{Cre/+}$ *Cd40*$^{fl/fl}$ mice had gene-expression signatures similar to those of their wild-type counterparts and retained the differences in gene expression previously reported between these two locations[36].

The defect in 1956-mOVA tumour rejection observed in *Xcr1*$^{Cre/+}$ *Cd40*$^{fl/fl}$ mice correlated with a greatly reduced expansion of endogenous CD8$^+$ T cells positive for the SIINFEKL-H-2K^b tetramer (Fig. 4c). In addition, CD40 expression by cDC1 was also required to support normal in vivo proliferation of OT-I T cells in response to immunization with cell-associated ovalbumin (Fig. 4d). By contrast, in vivo OT-I T cell proliferation was not reduced after transfer into tumour-bearing *Xcr1*$^{Cre/+}$ *Cd40*$^{fl/fl}$ mice compared to controls, nor after ex vivo co-culture with *Xcr1*$^{Cre/+}$ *Cd40*$^{fl/fl}$ cDC1 collected from tumour-draining lymph nodes compared with wild-type cDC1 (Extended Data Fig. 7c, d). These results suggest that CD40 on cDC1 is not required for initial antigen presentation during a tumour immune response. However, the number of OT-I CD8$^+$ T cells surviving three days after ex vivo co-culture with tumour-draining cDC1 was lower with *Xcr1*$^{Cre/+}$ *Cd40*$^{fl/fl}$ cDC1 than with controls (Fig. 4e). Together, these results suggest that CD40 signalling in cDC1 enhances the expansion and/or persistence of endogenous antigen-specific CD8$^+$ T cells during tumour rejection.

We next used in vivo OT-II proliferation to examine the effect of CD40 signalling in cDC1 on CD4$^+$ T cells, as that may alter CD4$^+$ T cell activation. After immunization with cell-associated ovalbumin, we observed substantially less in vivo OT-II proliferation in *Xcr1*$^{Cre/+}$ *Cd40*$^{fl/fl}$ mice than in wild-type (*Xcr1*$^{+/+}$ *Cd40*$^{fl/fl}$) mice (Fig. 4f). This difference was not seen after immunization with soluble ovalbumin (Extended Data Fig. 7e) or inoculation with 1956-mOVA tumours (Extended Data Fig. 7f). This result may be expected, as cDC2 present soluble ovalbumin to CD4$^+$ T cells and continue to express CD40 in *Xcr1*$^{Cre/+}$ *Cd40*$^{fl/fl}$ mice. Furthermore, the degree of OT-II proliferation occurring in *Xcr1*$^{Cre/+}$ *Cd40*$^{fl/fl}$ and wild-type mice is not comparable to that in the 1956-mOVA tumour system because the latter, but not the former, reject tumours, resulting in unequal antigen burdens. Nonetheless, immunization with equal amounts of cell-associated antigen (Fig. 4f) resulted in lower in vivo OT-II proliferation in mice lacking CD40 expression on cDC1.

Recent work suggests that CD4$^+$ T cells may act at the tumour site after priming to promote rejection[26], although the underlying mechanism is unclear. To examine this, we administered FTY720[37], a compound that blocks T cell exit from lymphoid organs, during both primary and secondary challenge with the 1956 fibrosarcoma cells (Extended Data Fig. 8a, b). However, FTY720 treatment reduced the emergence of both CD4$^+$ and CD8$^+$ T cells from lymphoid tissues (Extended Data Fig. 8c), making this approach inconclusive in interrogating the peripheral role of CD4$^+$ T cells. Nonetheless, we found that administration of FTY720 during either the primary or the secondary tumour challenge caused the failure of tumour rejection upon secondary challenge (Extended Data Fig. 8b, d, e). In addition, neither *Xcr1*$^{Cre/+}$ *MHCII*$^{fl/fl}$ nor *Xcr1*$^{Cre/+}$ *Cd40*$^{fl/fl}$ mice rejected secondary inoculation with

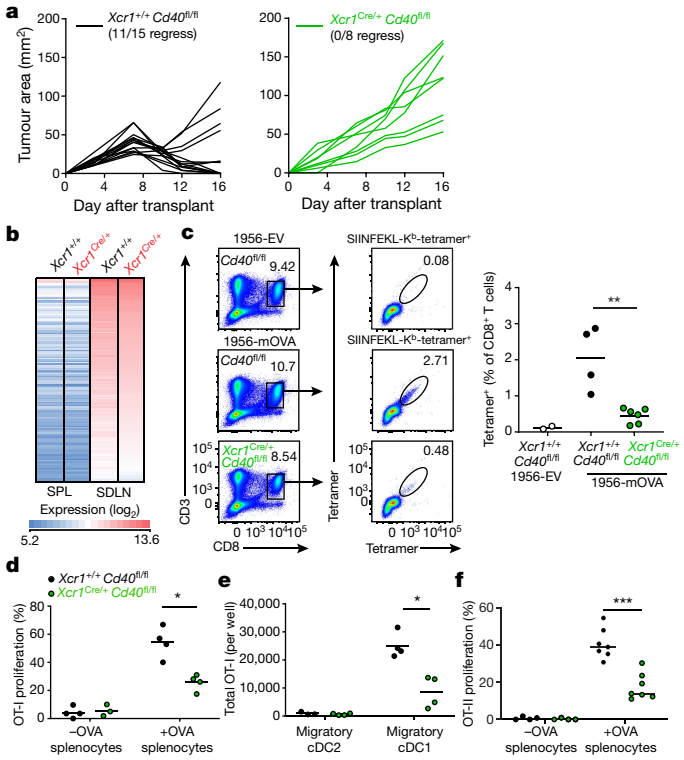

Fig. 4 | cDC1 expression of CD40 is required for tumour rejection. a, Tumour growth curves of *Xcr1*$^{+/+}$ *Cd40*$^{fl/fl}$ (left) and *Xcr1*$^{Cre/+}$ *Cd40*$^{fl/fl}$ mice (right) injected with 10^6 1956-mOVA. **b**, Log_2 expression of 148 genes with expression increased at least six-fold in skin-draining lymph node (SDLN) cDC1 relative to splenic (SPL) cDC1 (results averaged from biological triplicates). **c**, *Xcr1*$^{+/+}$ *Cd40*$^{fl/fl}$ and *Xcr1*$^{Cre/+}$ *Cd40*$^{fl/fl}$ mice were injected with 10^6 1956-EV or 1956-mOVA cells, and spleens were stained for the presence of SIINFEKL-K^b tetramer$^+$ CD8$^+$ T cells. Left, representative flow plots of percentages of tetramer$^+$ CD8 T cells. Right, tetramer$^+$ CD8$^+$ T cells as a percentage of all CD8$^+$ T cells. Data represent pooled biologically independent samples from two independent experiments ($n = 2$ for *Xcr1*$^{+/+}$ *Cd40*$^{fl/fl}$ 1956-EV, 4 for *Xcr1*$^{+/+}$ *Cd40*$^{fl/fl}$, 6 for *Xcr1*$^{Cre/+}$ *Cd40*$^{fl/fl}$). $^{**}P = 0.01$. **d**, Percentages of proliferated OT-I transferred into *Xcr1*$^{+/+}$ *Cd40*$^{fl/fl}$ and *Xcr1*$^{Cre/+}$ *Cd40*$^{fl/fl}$ mice immunized with cell-associated ovalbumin on day 0. Data are pooled independent samples from two independent experiments ($n = 3$ for *Xcr1*$^{Cre/+}$ *Cd40*$^{fl/fl}$ –OVA, $n = 4$ for all other groups). $^*P = 0.029$. **e**, Absolute numbers of proliferated OT-I per well after 72-h culture with ex vivo migratory cDC2 or cDC1 collected from tumour-draining lymph nodes of mice injected with 1956-mOVA. Data are pooled biologically independent samples from two independent experiments ($n = 3$ for *Xcr1*$^{+/+}$ *Cd40*$^{fl/fl}$ migratory cDC2, 4 for all other groups). $^*P = 0.029$. **f**, Percentages of proliferated OT-II transferred into *Xcr1*$^{+/+}$ *Cd40*$^{fl/fl}$ and *Xcr1*$^{Cre/+}$ *Cd40*$^{fl/fl}$ mice immunized with cell-associated ovalbumin on day 0. Data are pooled biologically independent samples from three independent experiments ($n = 4$ for –OVA groups, 7 for all other groups). $^{***}P = 0.006$. **c**–**f**: unpaired, two-tailed Mann–Whitney test.

the 1956 fibrosarcoma (Extended Data Fig. 8f, g). In lymph nodes, CD40 was expressed by migratory, but not resident, cDC1 (Extended Data Fig. 7a), as reported[36]. By contrast, we found very few cDC1 within the tumour microenvironment, where CD40 was expressed largely by B cells and macrophages (Extended Data Fig. 7g, h). These results suggest that CD40 signalling in cDC1 may have its primary effect in the lymph nodes, rather than at the tumour. Conceivably, the role of CD4$^+$ T cells in the tumour may be in activating tumour-associated macrophages, but this issue will require further study.

Finally, we used OT-I and OT-II T cells to examine the requirement for major histocompatibility classes I and II on cDC1 for entry into 1956-mOVA tumours (Extended Data Fig. 9). OT-I T cells entered tumours in wild-type mice, as expected, but not in *Xcr1*$^{Cre/+}$ *β2m*$^{fl/fl}$ mice (Extended Data Fig. 9a). By contrast, OT-I T cells entered tumours normally in *Xcr1*$^{Cre/+}$ *MHCII*$^{fl/fl}$ mice, but OT-II T cells did not (Extended Data Fig. 9b, c). Thus, notwithstanding the presence of other cells within the tumour expressing major histocompatibility class II molecules (Extended Data Fig. 7g), the entry of CD4$^+$ T cells into tumours seems to be sensitive to the relatively rare cDC1 in this location.

Discussion

Our results provide the first, to the best of our knowledge, in vivo demonstration that CD4$^+$ T cells must directly engage cDC1 via antigen–major histocompatibility class II interactions to induce cDC1-specific CD40 signalling required for optimal CD8$^+$ T cell responses. First, using *Irf8* +32$^{-/-}$ mice[30] that lack cDC1, we verified that cDC1 are exclusively responsible for priming anti-tumour CD8$^+$ T cells. We also, unexpectedly, found that in the context of tumour-derived antigens, cDC1 are also required for early priming of CD4$^+$ T cells. This result contrasts with previous models suggesting that CD4$^+$ T cells are initially activated by cDC2 and subsequently re-engage antigen–major histocompatibility class II molecules presented by cDC1 for licensing[5,12,38]. However, these models were based on studies indicating that cDC2 are superior in their processing of major histocompatibility class II antigens after the delivery of antigen to dendritic cells in vivo using antibodies[4,17,39]. Conceivably, the uptake and processing pathways of tumour-derived antigens may differ from those operating during their delivery via antibodies. For example, expression of the cDC1-specific receptor for filamentous actin, CLEC9A[40,41], may provide cDC1 with superior major histocompatibility class II processing in the context of tumour-derived antigens.

Naive CD4$^+$ T cells constitutively express intracellular CD40L[42] and so may immediately license cDC1 for CD8$^+$ T cell priming upon simultaneous presentation of tumour-derived antigens by major histocompatibility class I and II molecules. The possibility of non-cognate conventional dendritic cell licensing was suggested recently by an analysis of mice expressing transpeptidase sortase A fused to CD40L[43]. Twelve hours after immunization with peptide-loaded dendritic cells, enzymatic labelling of CD40 on dendritic cells required their expression of major histocompatibility class II, but after 48 hours it was independent of this[43]. However, that study did not test the functional consequences of these interactions. In our study, the loss of both major histocompatibility class II and CD40 caused a failure in the rejection of tumours, suggesting that functional interactions between CD4$^+$ T cells and cDC1 require cognate antigen recognition at some stage, although conceivably our model could incorporate late licensing via CD40 without cognate recognition.

Online content

Any methods, additional references, Nature Research reporting summaries, source data, extended data, supplementary information, acknowledgements, peer review information; details of author contributions and competing interests; and statements of data and code availability are available at https://doi.org/10.1038/s41586-020-2611-3.

1. Guilliams, M. et al. Dendritic cells, monocytes and macrophages: a unified nomenclature based on ontogeny. *Nat. Rev. Immunol.* **14**, 571–578 (2014).
2. Hildner, K. et al. Batf3 deficiency reveals a critical role for CD8α$^+$ dendritic cells in cytotoxic T cell immunity. *Science* **322**, 1097–1100 (2008).
3. Cancel, J. C., Crozat, K., Dalod, M. & Mattiuz, R. Are conventional type 1 dendritic cells critical for protective antitumor immunity and how? *Front. Immunol.* **10**, 9 (2019).
4. Dudziak, D. et al. Differential antigen processing by dendritic cell subsets in vivo. *Science* **315**, 107–111 (2007).
5. Binnewies, M. et al. Unleashing type-2 dendritic cells to drive protective antitumor CD4$^+$ T cell immunity. *Cell* **177**, 556–571 (2019).
6. Bennett, S. R., Carbone, F. R., Karamalis, F., Miller, J. F. & Heath, W. R. Induction of a CD8$^+$ cytotoxic T lymphocyte response by cross-priming requires cognate CD4$^+$ T cell help. *J. Exp. Med.* **186**, 65–70 (1997).
7. Bennett, S. R. et al. Help for cytotoxic-T-cell responses is mediated by CD40 signalling. *Nature* **393**, 478–480 (1998).

8. Schoenberger, S. P., Toes, R. E., van der Voort, E. I., Offringa, R. & Melief, C. J. T-cell help for cytotoxic T lymphocytes is mediated by CD40-CD40L interactions. *Nature* **393**, 480–483 (1998).
9. Bourgeois, C., Rocha, B. & Tanchot, C. A role for CD40 expression on $CD8^+$ T cells in the generation of $CD8^+$ T cell memory. *Science* **297**, 2060–2063 (2002).
10. Janssen, E. M. et al. $CD4^+$ T-cell help controls $CD8^+$ T-cell memory via TRAIL-mediated activation-induced cell death. *Nature* **434**, 88–93 (2005).
11. Williams, M. A., Tyznik, A. J. & Bevan, M. J. Interleukin-2 signals during priming are required for secondary expansion of $CD8^+$ memory T cells. *Nature* **441**, 890–893 (2006).
12. Borst, J., Ahrends, T., Bąbała, N., Melief, C. J. M. & Kastenmüller, W. $CD4^+$ T cell help in cancer immunology and immunotherapy. *Nat. Rev. Immunol*. **18**, 635–647 (2018).
13. Ridge, J. P., Di Rosa, F. & Matzinger, P. A conditioned dendritic cell can be a temporal bridge between a $CD4^+$ T-helper and a T-killer cell. *Nature* **393**, 474–478 (1998).
14. Smith, C. M. et al. Cognate $CD4^+$ T cell licensing of dendritic cells in $CD8^+$ T cell immunity. *Nat. Immunol*. **5**, 1143–1148 (2004).
15. Eickhoff, S. et al. Robust anti-viral immunity requires multiple distinct T Cell-dendritic cell interactions. *Cell* **162**, 1322–1337 (2015).
16. Hor, J. L. et al. Spatiotemporally distinct interactions with dendritic cell subsets facilitates $CD4^+$ and $CD8^+$ T cell activation to localized viral infection. *Immunity* **43**, 554–565 (2015).
17. Lehmann, C. H. K. et al. DC subset-specific induction of T cell responses upon antigen uptake via Fcγ receptors in vivo. *J. Exp. Med*. **214**, 1509–1528 (2017).
18. Bajaña, S., Roach, K., Turner, S., Paul, J. & Kovats, S. IRF4 promotes cutaneous dendritic cell migration to lymph nodes during homeostasis and inflammation. *J. Immunol*. **189**, 3368–3377 (2012).
19. Schlitzer, A. et al. IRF4 transcription factor-dependent $CD11b^+$ dendritic cells in human and mouse control mucosal IL-17 cytokine responses. *Immunity* **38**, 970–983 (2013).
20. Williams, J. W. et al. Transcription factor IRF4 drives dendritic cells to promote Th2 differentiation. *Nat. Commun*. **4**, 2990 (2013).
21. Valdez, Y. et al. Major histocompatibility complex class II presentation of cell-associated antigen is mediated by $CD8^{\alpha+}$ dendritic cells in vivo. *J. Exp. Med*. **195**, 683–694 (2002).
22. Theisen, D. J. et al. WDFY4 is required for cross-presentation in response to viral and tumor antigens. *Science* **362**, 694–699 (2018).
23. Sun, J. C. & Bevan, M. J. Defective CD8 T cell memory following acute infection without CD4 T cell help. *Science* **300**, 339–342 (2003).
24. Sun, J. C., Williams, M. A. & Bevan, M. J. $CD4^+$ T cells are required for the maintenance, not programming, of memory $CD8^+$ T cells after acute infection. *Nat. Immunol*. **5**, 927–933 (2004).
25. Matsushita, H. et al. Cancer exome analysis reveals a T-cell-dependent mechanism of cancer immunoediting. *Nature* **482**, 400–404 (2012).
26. Alspach, E. et al. MHC-II neoantigens shape tumour immunity and response to immunotherapy. *Nature* **574**, 696–701 (2019).
27. Bos, R. & Sherman, L. A. $CD4^+$ T-cell help in the tumor milieu is required for recruitment and cytolytic function of $CD8^+$ T lymphocytes. *Cancer Res*. **70**, 8368–8377 (2010).
28. Ferris, S. T. et al. A minor subset of Batf3-dependent antigen-presenting cells in islets of Langerhans is essential for the development of autoimmune diabetes. *Immunity* **41**, 657–669 (2014).
29. Theisen, D. J. et al. *Batf3*-dependent genes control tumor rejection induced by dendritic cells independently of cross-presentation. *Cancer Immunol. Res*. **7**, 29–39 (2019).
30. Durai, V. et al. Cryptic activation of an Irf8 enhancer governs cDC1 fate specification. *Nat. Immunol*. **20**, 1161–1173 (2019).
31. Srinivas, S. et al. Cre reporter strains produced by targeted insertion of EYFP and ECFP into the ROSA26 locus. *BMC Dev. Biol*. **1**, 4 (2001).
32. Bern, M. D. et al. Inducible down-regulation of MHC class I results in natural killer cell tolerance. *J. Exp. Med*. **216**, 99–116 (2019).
33. Hashimoto, K., Joshi, S. K. & Koni, P. A. A conditional null allele of the major histocompatibility IA-beta chain gene. *Genesis* **32**, 152–153 (2002).
34. Archambault, A. S. et al. Cutting edge: conditional MHC class II expression reveals a limited role for B cell antigen presentation in primary and secondary CD4 T cell responses. *J. Immunol*. **191**, 545–550 (2013).
35. Laidlaw, B. J., Craft, J. E. & Kaech, S. M. The multifaceted role of $CD4^+$ T cells in $CD8^+$ T cell memory. *Nat. Rev. Immunol*. **16**, 102–111 (2016).
36. Ardouin, L. et al. Broad and largely concordant molecular changes characterize tolerogenic and immunogenic dendritic cell maturation in thymus and periphery. *Immunity* **45**, 305–318 (2016).
37. Pinschewer, D. D. et al. FTY720 immunosuppression impairs effector T cell peripheral homing without affecting induction, expansion, and memory. *J. Immunol*. **164**, 5761–5770 (2000).
38. Ahrends, T. et al. $CD4^+$ T cell help confers a cytotoxic T cell effector program including coinhibitory receptor downregulation and increased tissue invasiveness. *Immunity* **47**, 848–861 (2017).
39. Kamphorst, A. O., Guermonprez, P., Dudziak, D. & Nussenzweig, M. C. Route of antigen uptake differentially impacts presentation by dendritic cells and activated monocytes. *J. Immunol*. **185**, 3426–3435 (2010).
40. Huysamen, C., Willment, J. A., Dennehy, K. M. & Brown, G. D. CLEC9A is a novel activation C-type lectin-like receptor expressed on $BDCA3^+$ dendritic cells and a subset of monocytes. *J. Biol. Chem*. **283**, 16693–16701 (2008).
41. Zhang, J. G. et al. The dendritic cell receptor Clec9A binds damaged cells via exposed actin filaments. *Immunity* **36**, 646–657 (2012).
42. Lesley, R., Kelly, L. M., Xu, Y. & Cyster, J. G. Naive CD4 T cells constitutively express CD40L and augment autoreactive B cell survival. *Proc. Natl Acad. Sci. USA* **103**, 10717–10722 (2006).
43. Pasqual, G. et al. Monitoring T cell-dendritic cell interactions in vivo by intercellular enzymatic labelling. *Nature* **553**, 496–500 (2018).

Methods

Generation of *Xcr1*-mCherry-hCre

Oligonucleotide primers used in the construction are described in Supplementary Table 1. The 3′ and 5′ homology arms were amplified by PCR from C57Bl/6 genomic DNA using Phusion High-Fidelity DNA polymerase (New England Biolabs, Inc.) using primers XCR1-5′ HA FOR and XCR1-5′ HA REV to generate a 5′ homology arm of 1,142 bp, and XCR1-3′ HA FOR and XCR1-3′ HA REV 2 to generate a 3′ homology arm of 5,495 bp. The vector backbone was amplified from the pENTR lox rNeo vector[44] as two overlapping fragments containing the attL2 and attL1 sites using the primers pENTR attL2 FOR and pENTR attL2 REV, and pENTR attL1 FOR and pENTR attL1 REV, respectively. The IRES was generated from the vector Spi-C-IRES-GFP[45] and the primers IRES pGK-Neo FOR and IRES pGK-Neo REV. An mCherry-Cre fragment was amplified from mCherry-T2A-hCre vector[46] using primers mCherry-T2A FOR and mCherry-T2A REV. Vector backbone, IRES and mCherry-Cre fragments were combined by Gibson assembly to generate the intermediate IRES-mCherry-T2A-hCre pENTR LoxP-Neo plasmid. A Frt-flanked rNeo fragment was produced by EcoRI digestion of pENTR FRT-rNeo[46] was inserted into this plasmid to make the intermediate IRES-mCherry-T2A-hCre pENTR Frt-rNeo. The 5′ and 3′ homology arms were sequentially inserted into this intermediate as SacI fragments. Finally, the plasmid containing the both homology arms was digested with PvuI, and a DTA fragment, amplified from pDEST-DTA-MLS[46] using primers pDEST DTA FOR and pDEST DTA REV, was inserted by Gibson assembly to yield the final IRES-mCherry-T2A-hCre targeting construct. The linearized targeting construct was electroporated into JM8.N4 ES cells, and targeted clones were screened by Southern blot analysis of SacI-digested genomic DNA. Correctly targeted clones were injected into blastocysts as described[46]. Southern probes were amplified using 5′ XCR1 FOR and 5′XCR1- REV and 3′XCR1 FOR and 3′XCR1 REV. Germline transmission and progeny genotype was assessed by PCR using the primers XCR1 IMC FOR, XCR1 IMC REV or XCR1 IMC IRES REV to generate amplicons of 165 bp (mutant) or 301 bp (wild type). The *Xcr1*-mCherry-hCre mouse is available at The Jackson Laboratory as Stock No. 035435.

Mice

Irf8 +32$^{-/-}$ mice, which are homozygous for the deletion of an downstream enhancer element of *Irf8*, were generated in house and described previously[30]. *IA*$_{\beta}{}^{b}$stop$^{f/f}$ (*MHCII*^{LSL})[34] mice were provided by G. Wu (Washington University, St Louis, MO). Mice harbouring floxed alleles of *β2-microglobulin* (*β2m*$^{fl/fl}$)[32] were provided by W. Yokoyama (Washington University, St Louis, MO). MHCI TKO mice (*Kb*$^{-/-}$*Db*$^{-/-}$*β2m*$^{-/-}$) were originally provided by T. Hansen (Washington University, St Louis, MO)[47]. C57Bl/6J (B6), *MHCII*^{fl} (B6.129X1-*H2-Ab1*^{tm1Koni}/J), C57Bl/6-Tg(TcraTcrb)1100Mb/J (OT-I), C57Bl/6-Tg(TcraTcrb)425Cbn/J (OT-II), B6.129X1-*Gt(ROSA)26Sor*$^{tm1(EYFP)Cos}$/J (R26^{LSLYFP}), B6.SJL-*Ptprc*^{a} *Pepc*^{b}*/BoyJ* (CD45.1), B6.129S2-*H2*$^{dlAb1\text{-}Ea}$/J (MHCII$^{-/-}$) and B6.129S4-*Gt(ROSA)26Sor*$^{tm1(FLP1)Dym}$/RainJ (R26^{FLP}) mice were purchased from The Jackson Laboratory. CD45.1 mice were bred to OT-I and OT-II mice to produce CD45.1 OT-I and CD45.1 OT-II, respectively. The Cd40$^{tm1a(KOMP)Wtsi}$ mouse used for this project was generated by the trans-NIH Knock-Out Mouse Project (KOMP) and obtained from the KOMP Repository (www.komp.org). NIH grants to Velocigene at Regeneron Inc (U01HG004085) and the CSD Consortium (U01HG004080) funded the generation of gene-targeted ES cells for 8,500 genes in the KOMP Program and archived and distributed by the KOMP Repository at UC Davis and CHORI (U42RR024244). The Cd40$^{tm1a(KOMP)Wtsi}$ trapping cassette "SA-βgeo-pA" (splice acceptor-beta-geo-polyA) flanked by Flp-recombinase target FRT sites was converted to a conditional allele by breeding to R26^{FLP} mice. The resulting mice lack the gene trap cassette, leaving two *loxP* sites flanking exons 2–4 of *Cd40* (*Cd40*^{fl}). The resultant *Cd40*^{fl} mice were subsequently used in experiments where indicated. *Xcr1*^{Cre} mice with germline deletion of major histocompatibility complex class I (MHCI), MHCII or CD40 were excluded from our study.

All in vivo experiments were performed in our specific-pathogen free facility and both sexes were used between the ages of 8 and 16 weeks. All animals were maintained on 12-hour light cycles and housed at 70 °F (~21 °C and 50% humidity. All experiments were performed in accordance with procedures approved by the AAALAC-accredited Animal Studies Committee of Washington University in St Louis and were in compliance with all relevant ethical regulations.

Tumour lines and growth experiments

The methylcholanthrene (MCA)-induced fibrosarcoma 1956 was a gift from Robert Schreiber (Washington University School of Medicine). It was generated in a female C57Bl/6 mouse, tested for mycoplasma, and banked at low passage as previously described[25]. The B16F10 (ATCC® CRL6475™) melanoma was purchased from ATCC. Tumour cells derived from frozen stocks were propagated for 1 week with one intervening passage in vitro in Iscove's modified Dulbecco's media (IMDM) or RPMI media supplemented with 10% FCS (HyClone), washed three times with PBS and resuspended at a density of 6.67×10^6 cells/mL in endotoxin-free PBS. Mice were subcutaneously injected into the flanks with 10^6 tumour cells. Tumour growth was measured with a calliper, and tumour area was calculated by the multiplication of two perpendicular diameters. In accordance with our IACUC-approved protocol, maximal tumour diameter was 20 mm in one direction, and in no experiments was this limit exceeded.

For tumour memory experiments, 10^6 1956 cells were injected subcutaneously into C57Bl/6 mice. Tumours were resected after 8 d. A further 30 d later, 10^6 1956 cells were injected subcutaneously into the contralateral flanks. For T cell depletions, 250 μg of depleting CD4 (YTS 191.1) or CD8 (YTS 169.4) antibodies (BioXcell) was injected intraperitoneally (IP) on day −4 and day 0 during the primary response or injected IP on day 34 and day 38 during the secondary response. For treatment with FTY720 (Sigma-Aldrich), a stock concentration of 5 mg/mL in DMSO was diluted to 125 μg/mL in PBS directly before injection. Mice were injected IP with 25 μg FTY720 or PBS/DMSO on day −1 and every subsequent 3 d during the primary response, or injected IP on day 37 and every subsequent 3 d during the secondary response.

An immunogenic fibrosarcoma expressing membrane ovalbumin was generated from the MCA-induced progressor fibrosarcoma 1956 (1956-mOVA). The mOVA fragment isolated from pCI-neo-mOVA (Addgene #25099) was ligated into the MSCV-IRES-Thy1.1 vector[48] to generate MSCV-mOVA-IRES-Thy1.1. 1956 tumour cells were retrovirally transduced with this vector and were sorted for expression of Thy1.1. Individual clones of 1956-mOVA were generated by limited dilution cloning and were tested for growth in C57Bl/6 mice. Clone 1 was selected by expression of Thy1.1 and surface OVA (Millipore AB1225) using flow cytometry. The control fibrosarcoma expressing Thy1.1 (1956-EV) was generated from 1956 by retroviral transduction of the MSCV-IRES-Thy1.1 vector. Individual clones of 1956-EV were generated by limited dilution cloning and were tested for growth in C57Bl/6 mice. Clone 3 was selected by expression of Thy1.1 using flow cytometry. The B16F10 melanoma was engineered to express membrane ovalbumin using the same MSCV-mOVA-IRES-Thy1.1 vector. B16F10 tumour cells were retrovirally transduced with this vector and were sorted for expression of Thy1.1. However, over time in culture, the cells lost expression of Thy1.1 but retained expression of mOVA. Clone 2 was selected by expression of surface OVA (Millipore AB1225) using flow cytometry. Bulk B16F10 cells transduced with MSCV-IRES-Thy1.1 (B16F10-EV) were used as control tumour cells.

Dendritic cell preparation

Lymphoid and non-lymphoid organ dendritic cells were harvested and prepared as described previously[30]. Briefly, spleens and inguinal

skin-draining lymph nodes were minced and digested in 5 ml of IMDM + 10% FCS (cIMDM) with 250 μg/ml of collagenase B (Roche) and 30 U/ml of DNaseI (Sigma-Aldrich) for 45 min at 37 °C with stirring. Tumours were minced and digested in serum-free IMDM with 125 μg/ml Liberase (Roche) and 30 U/mL of DNaseI (Sigma-Aldrich) for 45 minutes at 37 °C with stirring. After digestion was complete, single-cell suspensions from all organs were passed through 70-μm strainers and red blood cells were lysed with ammonium chloride–potassium bicarbonate (ACK) lysis buffer. Cells were subsequently counted with a Vi-CELL analyser (Beckman Coulter), and 3–5 × 10^6 cells were used per antibody staining reaction.

Soluble and cell-associated T cell proliferation assay

CD45.1 OT-II TCR transgenic mouse lymph nodes and spleens were harvested and dispersed into single-cell suspensions by mechanical separation. Cells were then stained with biotinylated Ter119, CD8b, I-A/I-E and Ly6G antibodies for 20 min at 4 °C. CD45.1 OT-I TCR transgenic mouse lymph nodes and spleens were harvested and dispersed into single-cell suspensions by mechanical separation. Cells were then stained with biotinylated Ter119, CD4, I-A/I-E and Ly6G antibodies for 20 min at 4 °C. Cells were washed incubated with MagniSort™ SAV negative selection beads (Invitrogen) according to manufacturer's protocol. Cells were magnetically separated and sorted as B220$^-$ CD8$^-$ TCRβ$^+$ CD4$^+$ CD45.1$^+$ Vα2$^+$ (OT-II) or as B220$^-$ CD8$^+$ TCRβ$^+$ CD4$^-$ CD45.1$^+$ Vα2$^+$ (OT-I). Cells were labelled with either 1 μM CFSE or Cell Trace Violet (Thermo Fisher Scientific) proliferation dyes. Labelled OT-I cells (5 × 10^5) or OT-II cells (10^6) were transferred intravenously into mice 1 d before immunization with 100 μg of either soluble or cell-associated OVA. Cell-associated OVA was produced by isolating either MHCI TKO splenocytes (OT-I proliferation assays) or *MHCII*$^{LSL/-}$ splenocytes (OT-II proliferation assays) and osmotically loading with 10 mg/ml soluble ovalbumin (Worthington Biochemical Corporation). Cells were irradiated at 1,350 rad, and 5 × 10^5 MHCI TKO cells or 2 × 10^6 *MHCII*$^{LSL/-}$ cells were injected intravenously into mice. After 3 d, spleens were harvested, mashed and analysed for proliferation dye dilution of transferred CD45.1 OT-I or OT-II cells.

CD8$^+$ T cell tetramer staining

Spleens were harvested 10 d after tumour transplantation, digested in collagenase B (0.25 mg/mL) and DNaseI (30 U/mL) in complete IMDM (Iscove's modified Dulbecco's medium with 10% FCS, 2ME, penicillin/streptomycin, NEAA and glutamine) for 40 min at 37 °C with stirring and subjected to ACK lysis. SIINFEKL-H2-K^b biotinylated monomers were purchased from the immunomonitoring core lab at the Bursky Center for Human Immunology and Immunotherapy Programs. The peptide–MHC class I complexes refolded with an ultraviolet-cleavable conditional ligand were prepared as described with modifications[49]. Briefly, recombinant the H-2K^b heavy chain and the human β2 microglobulin light chain were produced in *Escherichia coli*, isolated as inclusion bodies and dissolved in 4 M urea, 20 mM Tris, pH 8.0. MHC class I refolding reactions were performed by dialyzing a molar ratio of heavy chain:light chain:peptide of 1:1:8 against 10 mM potassium phosphate, pH 7.4, for 48 h. Refolded peptide–MHC class I complexes were captured by ion exchange (HiTrap Q HP, GE), biotinylated and purified by gel filtration FPLC. Ultraviolet-induced ligand exchange and combinatorial encoding of MHC class I multimers was performed as described[50]. Then, the peptide–MHC multimers were incubated with BV605- and BV710-conjugated streptavidin (SA) at a concentration of 1:5 for 30 min at 4 °C protected from light in separate reactions. SA-labelled tetramers were then incubated with 25 μM D-biotin for 20 min at 4 °C protected from light to quench free fluorochrome-labelled SA. 3 × 10^6 splenocytes were incubated with 10% BSA, 2 mM EDTA phosphate buffered saline (PBS) supplemented with 10% of supernatant containing the Fc-blocking antibody produced from the 2.4G2 cell line for 5 min at 4 °C. Fluorochrome-conjugated tetramers were added to the splenocytes at a concentration of 3:50 and incubated at 37 °C for 30 min. Surface antibodies were added without washing and stained for another 30 min at 4 °C.

Tumour-specific in vivo T cell priming assay

CD45.1 OT-II or OT-I TCR transgenic cells were isolated as stated above. Cells were washed incubated with MagniSort™ SAV negative selection beads (Invitrogen) according to manufacturer's protocol. Cells were magnetically separated and sorted as B220$^-$ CD8$^-$ TCRβ$^+$ CD4$^+$ CD45.1$^+$ Vα2$^+$ (OT-II) or B220$^-$ CD8$^+$ TCRβ$^+$ CD4$^-$ CD45.1$^+$ Vα2$^+$ (OT-I). Cells were labelled with either 1 μM CFSE or Cell Trace™ Violet (Thermo Fisher Scientific) proliferation dyes. One million labelled OT-II or OT-I cells were transferred intravenously into mice on day 2 after tumour implantation. Tumour draining lymph nodes were harvested on day 5 after tumour implantation (3 d after T cell transfer) and assayed for dye dilution. Tumours were harvested on day 5 or day 7 after implantation (3 or 5 d after T cell transfer) and assayed for accumulation as a percentage of total CD45$^+$ cells.

Expression microarray analysis

Xcr1$^{+/+}$ and *Xcr1*$^{Cre/+}$*Cd40*$^{fl/fl}$ spleens and skin-draining lymph nodes were harvested and digested in collagenase B (0.25 mg/mL) and DNaseI (30 U/mL) in complete IMDM (Iscove's modified Dulbecco's medium with 10% FCS, 2ME, penicillin/streptomycin, NEAA, and glutamine) for 40 min at 37 °C with stirring. Cells were then stained with biotinylated CD3, CD19, Ter119 and Ly6G antibodies for 20 min at 4 °C. Cells were washed and then incubated with MagniSort™ SAV negative selection beads (Invitrogen) according to manufacturer's protocol. After magnetic depletion, cells were sorted as B220$^-$ MHCII^{hi} CD11c^{int} XCR1$^+$ CD172α$^-$. RNA from sorted dendritic cell populations was extracted with a NucleoSpin RNA XS Kit (Macherey-Nagel), amplified with WT Pico System (Affymetrix, Inc.) and hybridized to GeneChip Mouse Gene 1.0 ST microarrays (Affymetrix, Inc.) for 18 h at 45 °C in a GeneChip Hybridization Oven 640. The data were analysed using the Affymetrix GeneChip Command Console. Microarray expression data were processed using Command Console (Affymetrix, Inc.), and the raw (.CEL) files generated were analysed using Expression Console software with Affymetrix default Robust Multichip Analysis Gene analysis settings (Affymetrix, Inc.). Probe summarization (Robust Multichip Analysis), quality control analysis and probe annotation were performed according to recommended guidelines (Expression Console Software, Affymetrix, Inc.). Data were normalized by robust multiarray average summarization and underwent quantile normalization with ArrayStar software (DNASTAR).

Ex vivo tumour-draining dendritic cell co-culture–T cell priming assay

Mice were injected subcutaneously with 2 × 10^6 1956-mOVA cells on each flank. On day 6 after tumour implantation, tumour-draining lymph nodes were harvested and digested in collagenase B (0.25 mg/mL) and DNaseI (30 U/mL) in complete IMDM (Iscove's modified Dulbecco's medium with 10% FCS, 2ME, penicillin/streptomycin, NEAA and glutamine) for 40 min at 37 °C with stirring. Cells were then stained with biotinylated CD3, CD19, Ter119 and Ly6G antibodies for 20 min at 4 °C. Cells were washed and then incubated with MagniSort™ SAV negative selection beads (Invitrogen) according to manufacturer's protocol. After magnetic depletion, cells were sorted as migratory cDC1 (B220$^-$ MHCII^{hi} CD11c^{int} XCR1$^+$ CD172α$^-$) or migratory cDC2 (B220$^-$ MHCII^{hi} CD11c^{int} XCR1$^-$ CD172α$^+$) into I10F. CD45.1 OT-I TCR transgenic cells were isolated as stated above. Cells were washed incubated with MagniSort™ SAV negative selection beads (Invitrogen) according to manufacturer's protocol. Cells were magnetically separated and sorted as B220$^-$ CD8$^+$ TCRβ$^+$ CD4$^-$ CD45.1$^+$ Vα2$^+$ CD44^{lo} CD62L^{hi}. Cells were labelled with either 1 μM CFSE or Cell Trace Violet (Thermo Fisher Scientific) proliferation dyes. OT-I cells were co-cultured in complete IMDM with migratory cDC1 or cDC2 at a ratio of 10:1 in 96-well round-bottom plate (Corning)

at 37 °C. After 72 h, cells were washed and stained with antibodies for evaluation of proliferation and expansion.

Antibodies and flow cytometry

Flow cytometry and cell sorting were completed on a FACS CantoII or FACS Aria Fusion instrument (BD) and analysed using FlowJo analysis software (Tree Star). Staining was performed at 4 °C in the presence of Fc block (2.4G2) in magnetic-activated cell-sorting (MACS) buffer (PBS + 0.5% BSA + 2 mM EDTA). The following antibodies were used; from BD Biosciences: CD117 (2B8), CD135 (A2F10.1), Ly6C (AL-21), MHCI (AF6-88.5), CD4 (RM4-5), CD8α (53-6.7), CD8β (53-5.8), CD11b (M1/70), B220 (RA3-6B2), CD64 (X54-5/7.1), CD19 (1D3), CD95 (Jo2), CD3 (145-2C11), CD45 (30-F11); from Tonbo Biosciences: MHCII (M5/114.15.2), CD44 (IM7), CD45.1 (A20), CD45.2 (104), CD11c (N418); from Biolegend: SA-BV605, SA-711, CCR7 (4B12), CD103 (2E7), XCR1 (ZET), CD115 (AFS98), Ter119 (Ter-119), Ly6G (1A8), TCRβ (H57-597), CD3 (145-2C11), CD8 (53-6.7), CD4 (RMA4-5), CD44 (IM7), CD40 (1C10), CD16/32 (93); from eBiosciences: TCRVα2 (B20.1), CD45.1 (A20), CD90.1 (HIS51), CD90.2 (53-2.1), F4/80 (BM8); from Invitrogen: CD172α (P84), CD45 (30F11); from Millipore/Sigma: rabbit anti-ovalbumin (AB1225).

Statistics

Statistical analysis was performed using GraphPad Prism software version 8. Unless otherwise noted, Mann–Whitney *U* test was used to determine significant differences between samples, and all centre values correspond to the mean. No formal randomization was performed as comparisons were done across mice of different genotypes, not across mice of the same genotypes receiving different treatments. No formal randomization was done across all other samples. Investigators were blinded to the genotype of the mice during sample preparation and data collection.

Reporting summary

Further information on research design is available in the Nature Research Reporting Summary linked to this paper.

Data availability

The microarray data generated during the course of this study have been deposited and are available at the Gene Expression Omnibus (GEO) database. The microarrays used in Fig. 4b and Extended Data Fig. 7b can be accessed with the accession number GSE152196. All other primary data and materials that support the findings of this study are available from the corresponding author upon request. Source data are provided with this paper.

44. Satpathy, A. T. et al. Zbtb46 expression distinguishes classical dendritic cells and their committed progenitors from other immune lineages. *J. Exp. Med.* **209**, 1135–1152 (2012).
45. Kohyama, M. et al. Role for Spi-C in the development of red pulp macrophages and splenic iron homeostasis. *Nature* **457**, 318–321 (2009).
46. Wu, X. et al. Mafb lineage tracing to distinguish macrophages from other immune lineages reveals dual identity of Langerhans cells. *J. Exp. Med.* **213**, 2553–2565 (2016).
47. Lybarger, L., Wang, X., Harris, M. R., Virgin, H. W., IV & Hansen, T. H. Virus subversion of the MHC class I peptide-loading complex. *Immunity* **18**, 121–130 (2003).
48. Sedy, J. R. et al. B and T lymphocyte attenuator regulates T cell activation through interaction with herpesvirus entry mediator. *Nat. Immunol.* **6**, 90–98 (2005).
49. Toebes, M. et al. Design and use of conditional MHC class I ligands. *Nat. Med.* **12**, 246–251 (2006).
50. Andersen, R. S. et al. Parallel detection of antigen-specific T cell responses by combinatorial encoding of MHC multimers. *Nat. Protocols* **7**, 891–902 (2012).

Acknowledgements K.M.M. was supported by the Howard Hughes Medical Institute and the US National Institutes of Health (R01AI150297); R.D.S. by grants from the National Institutes of Health (R01CA190700) and The Parker Institute for Cancer Immunotherapy, and a Stand Up To Cancer–Lustgarden Foundation Pancreatic Cancer Foundation Convergence Team Translational Research Grant; W.M.Y. by a grant from the National Institutes of Health (R01AI129545); M.D.B. and V.D. by fellowship grants from the National Institutes of Health (F30DK112466 and F30DK108498, respectively); S.T.F. by a postdoctoral training grant from the National Institutes of Health (T32CA95473); G.F.W., D.J.T. and J.T.D. by the National Institutes of Health (R01NS106289, T32 AI007163 and T32CA009621, respectively); and P.B. by the US National Science Foundation (DGE-1143954). We thank the Genome Technology Access Center, Department of Genetics, Washington University School of Medicine in St Louis, for help with genomic analysis. The Center is supported by Cancer Center Support Grant P30 CA91842 from the US National Cancer Institute and by Institute of Clinical and Translational Sciences/Clinical and Translational Science Award UL1 TR000448 from the US National Center for Research Resources. Aspects of studies including tetramer production were performed with assistance by the Immunomonitoring Laboratory, which is supported by the Andrew M. and Jane M. Bursky Center for Human Immunology and Immunotherapy Programs and the Alvin J. Siteman Comprehensive Cancer Center that, in turn, is supported by the National Cancer Institute of the National Institutes of Health Cancer Center Support Grant (P30CA91842) and the Washington University Rheumatic Diseases Research Resource-based Center Grant (P30AR073752).

Author contributions S.T.F., R.W. and V.D. conceived and designed the experiments, collected the data, and performed and interpreted the analyses. S.T.F. and R.W. wrote the manuscript. J.T.D., P.B., D.J.T., T.L., L.L. and C.G.B. collected and analysed data. J.P.W. and D.J.T. helped generate the 1956-mOVA fibrosarcoma cell line. M.D.B. provided the *β2m*$^{fl/fl}$ mouse and interpreted the analyses. G.F.W., W.M.Y., W.E.G., T.L.M. and R.D.S. provided assistance with experimental design. K.M.M. conceived experiments, interpreted data, and wrote the manuscript.

Competing interests R.D.S. is a cofounder, scientific advisory board member, stockholder and royalty recipient of Jounce Therapeutics and Neon Therapeutics and is a scientific advisory board member for A2 Biotherapeutics, BioLegend, Codiak Biosciences, Constellation Pharmaceuticals, NGM Biopharmaceuticals and Sensei Biotherapeutics.

Additional information
Supplementary information is available for this paper at https://doi.org/10.1038/s41586-020-2611-3.
Correspondence and requests for materials should be addressed to K.M.M.
Peer review information *Nature* thanks Cornelis Melief, Sebastian Amigorena and the other, anonymous, reviewer(s) for their contribution to the peer review of this work.
Reprints and permissions information is available at http://www.nature.com/reprints.

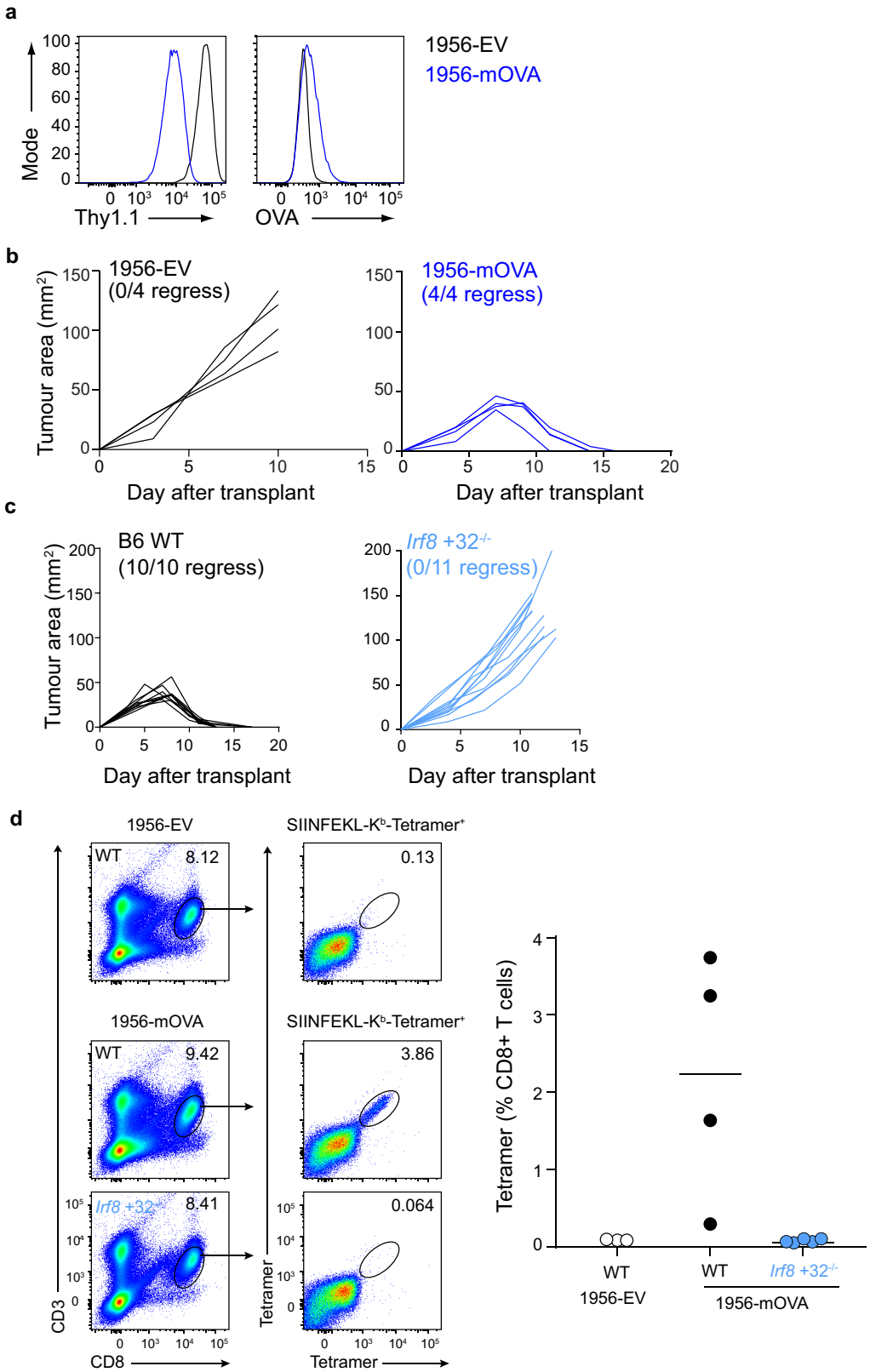

Extended Data Fig. 1 | cDC1 are required to prime CD4⁺ T cells during the tumour immune response. a, 1956-EV and 1956-mOVA were stained with antibodies against (left) Thy1.1 and (right) OVA. **b**, Tumour growth curves of B6 wild-type (WT) mice injected with 10^6 (left)1956-EV or (right)1956-mOVA. **c**, Tumour growth curves of (left) B6 WT or (right) *Irf8* +32$^{-/-}$ mice injected with 10^6 1956-mOVA. **d**, B6 WT or *Irf8* +32$^{-/-}$ mice were subcutaneously injected with 10^6 1956-EV or 10^6 1956-mOVA. Spleens were isolated and stained for presence of SIINFEKL-K^b-tetramer$^+$ CD8$^+$ T cells. (Left) Representative flow plots of percentage of tetramer$^+$ CD8$^+$ T cells. (Right) Graph of tetramer$^+$ CD8$^+$ T cells as a percentage of all T cells. Data are pooled biologically independent samples from two independent experiments ($n = 3$ for WT EV, $n = 4$ for WT 1956-mOVA, $n = 5$ for *Irf8* +32$^{-/-}$ 1956-mOVA).

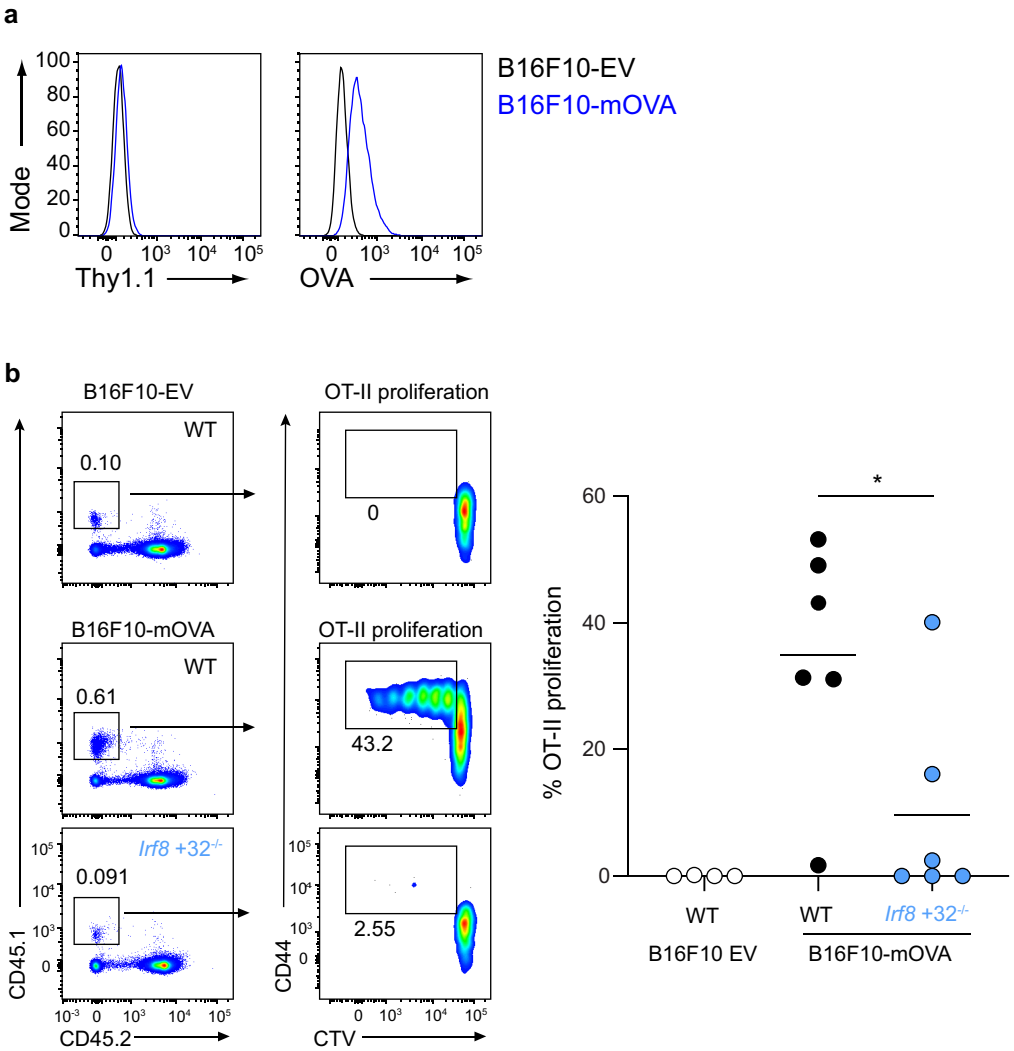

Extended Data Fig. 2 | cDC1 are required to prime CD4$^+$ T cells during the immune response to B16F10 melanoma. a, B16F10-EV and B16F10-mOVA were stained with antibodies against (left) Thy1.1 and (right) OVA. **b**, B6 WT or *Irf8* +32$^{-/-}$ mice were subcutaneously injected with 10^6 B16F10-EV or 10^6 B16F10-mOVA. (Left) Representative flow plots of OT-II T cells 3 days after transfer. (Right) Graph of per cent proliferated OT-II transferred. Data are pooled biologically independent samples from two independent experiments ($n = 4$ for WT B16F10-EV, $n = 6$ for all other groups).*$P = 0.04$ (unpaired, two-tailed Mann–Whitney test).

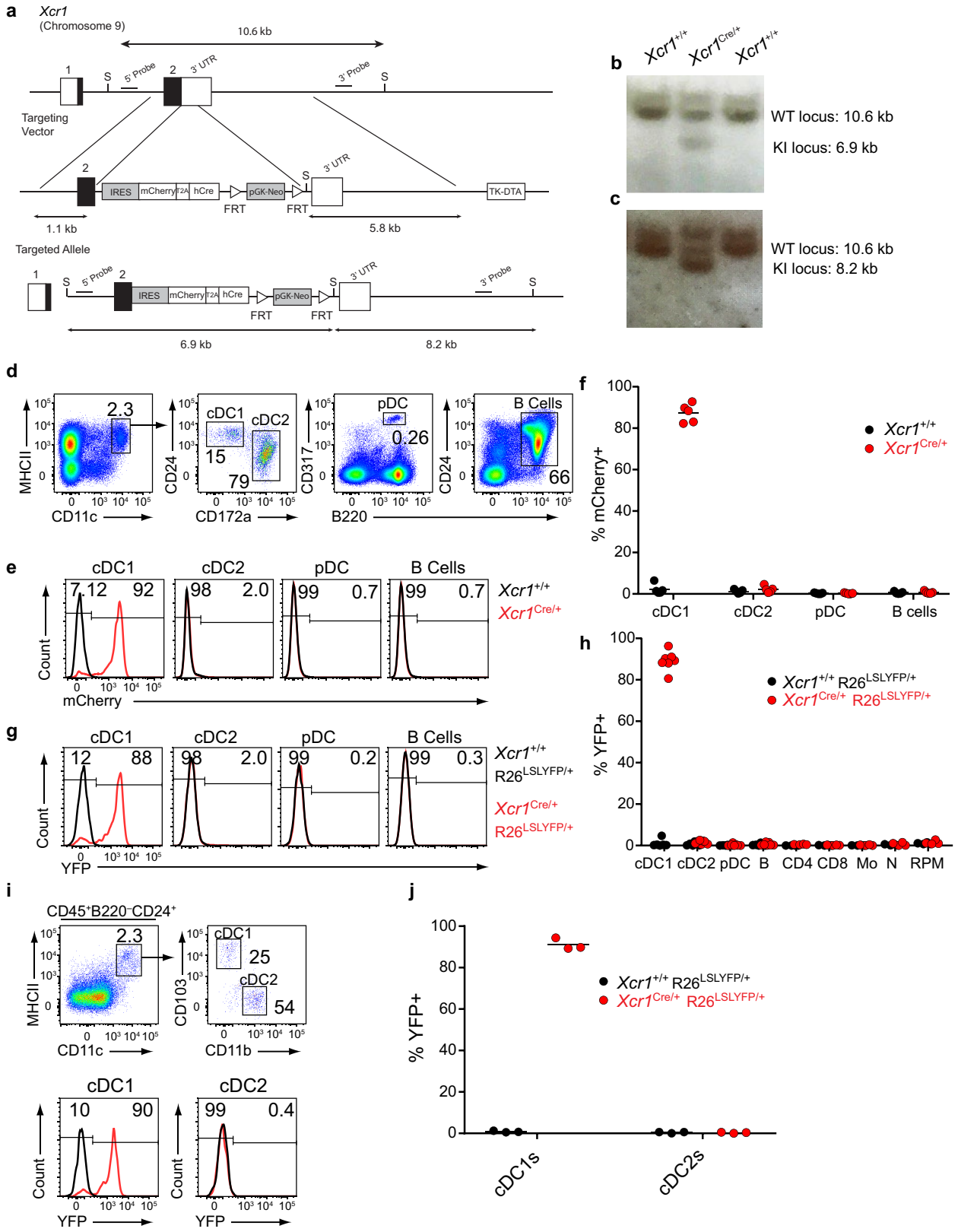

Extended Data Fig. 3 | See next page for caption.

Extended Data Fig. 3 | Validation of mCherry expression and lineage tracing of *Xcr1*^{Cre} mouse. a, Schematic diagrams of the mouse *Xcr1* WT allele, the targeting vector (IRES-mCherry-T2a-hCRE with FRT flanked pGK-Neo cassettes), and the targeted allele. Filled and open boxes denote coding and noncoding exons of *Xcr1*, respectively. **b**, Southern blot analysis of *Xcr1*$^{+/+}$ and *Xcr1*$^{Cre/+.}$ Genomic DNAs were isolated from mice tails, digested with SalI, electrophoresed, and hybridized with the 5′-radiolabelled probe indicated in **a**. Southern blot gave a 10.6 and a 6.9 kbp band for WT and targeted allele, respectively. For Southern blot source data, see Supplementary Fig. 1. **c**, Southern blot analysis of *Xcr1*$^{+/+}$ and *Xcr1*$^{Cre/+}$. Genomic DNAs were isolated from mice tails, digested with SalI, electrophoresed, and hybridized with the 3′ radiolabelled probe indicated in **a**. Southern blot gave a 10.6 and a 8.2 kbp band for WT and targeted allele, respectively. For Southern blot source data, see Supplementary Fig. 1. **d**, Gating strategy to delineate splenic cell populations. **e**, FACs histograms of mCherry expression from subpopulations in **d** isolated from *Xcr1*$^{Cre/+}$ and *Xcr1*$^{+/+}$ mice. **f**, Graph of mCherry expression in antigen-presenting cell populations gated from **d** isolated from *Xcr1*$^{Cre/+}$ and *Xcr1*$^{+/+}$ mice. Data are pooled biologically independent samples from two independent experiments ($n = 5$ in all groups). **g**, FACs histograms for YFP expression from subpopulations in **d** isolated from *Xcr1*$^{Cre/+}$ R26$^{LSLYFP/+}$ and *Xcr1*$^{+/+}$ R26$^{LSLYFP/+}$ mice. **h**, Graph of YFP expression in splenic cell populations (Mo, monocytes; N, neutrophils; RPM, red pulp macrophages). Data are pooled biologically independent samples from two independent experiments ($n = 6$ for cDC1, cDC2, plasmacytoid dendritic cells (pDC) and B cells from *Xcr1*$^{+/+}$ R26$^{LSLYFP/+}$ mice, $n = 7$ for cDC1, cDC2, pDC and B cells from *Xcr1*$^{Cre/+}$ R26$^{LSLYFP/+}$ mice, and $n = 4$ for all other groups). **i**, (Top) Gating strategy to delineate SDLN cell populations. (Bottom) FACs histograms for YFP expression in cDC1 and cDC2 isolated from *Xcr1*$^{Cre/+}$ R26$^{LSLYFP/+}$ and *Xcr1*$^{+/+}$ R26$^{LSLYFP/+}$ mice. **j**, Graph of YFP expression from subpopulations in **i** isolated from *Xcr1*$^{Cre/+}$ R26$^{LSLYFP/+}$ and *Xcr1*$^{+/+}$ R26$^{LSLYFP/+}$ mice. Data are pooled biologically independent samples from two independent experiments ($n = 3$ in all groups).

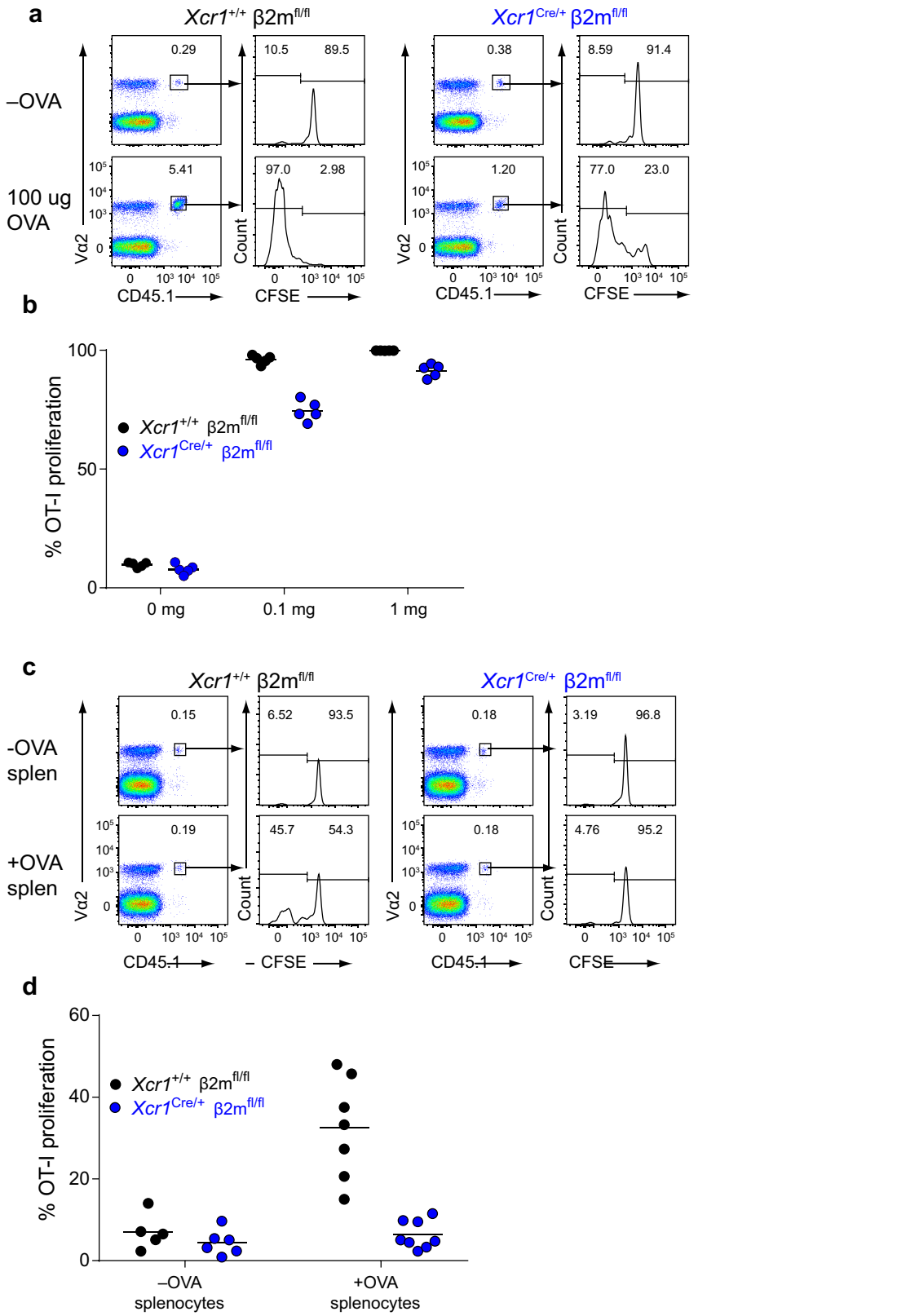

Extended Data Fig. 4 | Proliferation of OT-I in *Xcr1*$^{Cre/+}$ *β2m*$^{fl/fl}$ mice receiving soluble or cell-associated OVA. a, Representative FACs analysis and histograms of CFSE dilution of proliferated OT-I on day 3 after transfer into (left) *Xcr1*$^{+/+}$ *β2m*$^{fl/fl}$ and (right) *Xcr1*$^{Cre/+}$ *β2m*$^{fl/fl}$ immunized with soluble OVA. **b**, Graph of per cent proliferation of transferred OT-I in mice immunized with soluble OVA. Data are pooled biologically independent samples from two independent experiments ($n = 5$ for all groups). **c**, Representative FACs analysis and histograms of CFSE dilution of proliferated OT-I on day 3 after transfer into (left) *Xcr1*$^{+/+}$ *β2m*$^{fl/fl}$ and (right) *Xcr1*$^{Cre/+}$ *β2m*$^{fl/fl}$ immunized with cell-associated OVA. **d**, Graph of per cent proliferation of transferred OT-I in mice immunized with cell-associated OVA. Data are pooled biologically independent samples from two independent experiments ($n = 5$ *Xcr1*$^{+/+}$ *β2m*$^{fl/fl}$ –OVA, $n = 6$ for *Xcr1*$^{Cre/+}$ *β2m*$^{fl/fl}$ +OVA, $n = 7$ for *Xcr1*$^{+/+}$ *β2m*$^{fl/fl}$ +OVA, and $n = 8$ for *Xcr1*$^{Cre/+}$ *β2m*$^{fl/fl}$ +OVA).

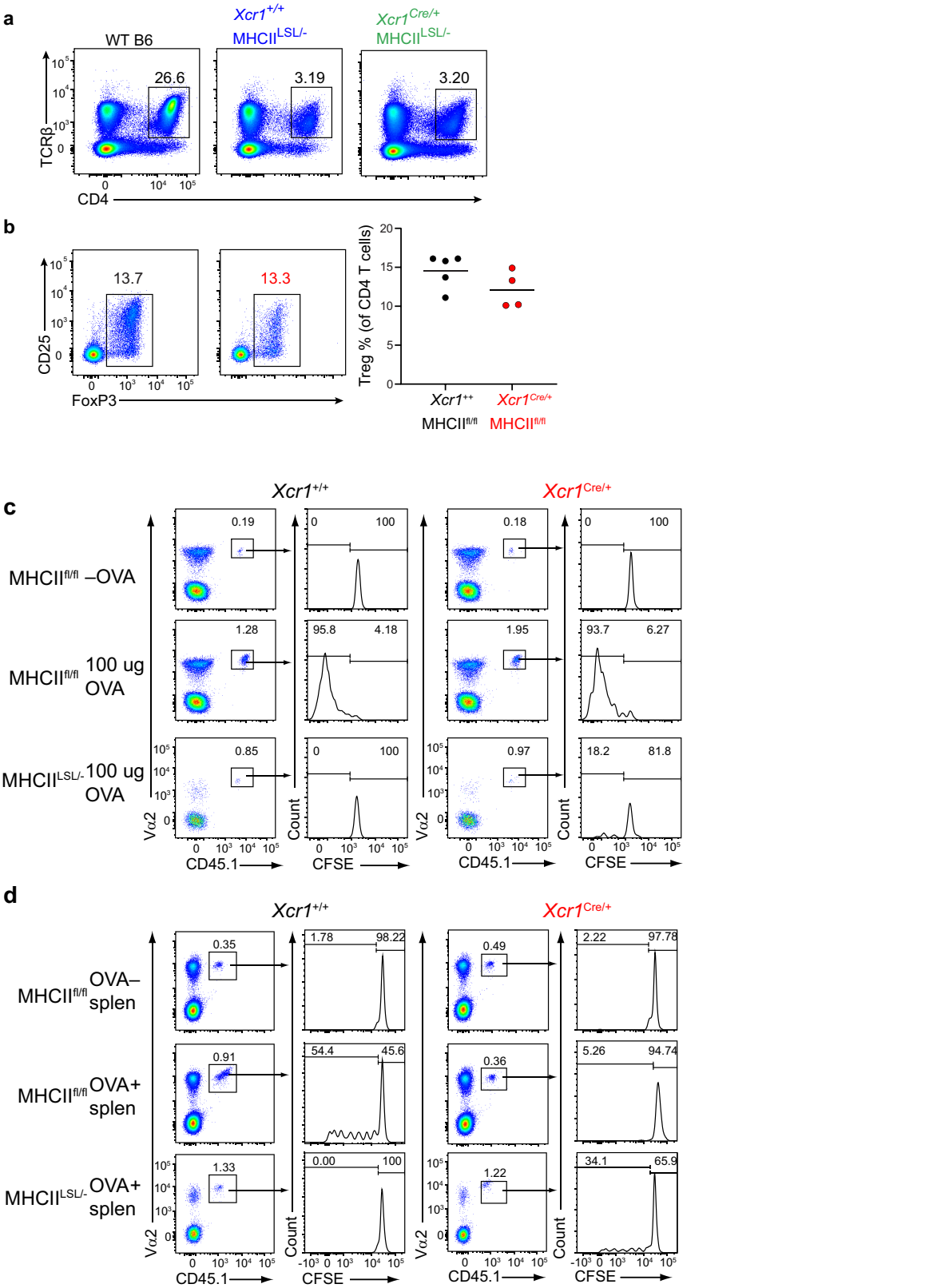

Extended Data Fig. 5 | Proliferation of OT-II in *Xcr1*$^{Cre/+}$ *MHCII*$^{fl/fl}$ and *Xcr1*$^{Cre/+}$ *MHCII*$^{LSL/-}$ mice immunized with soluble and cell-associated OVA. **a**, Representative FACS analysis of splenic CD4$^+$ T cell percentage in WT B6, *Xcr1*$^{+/+}$ *MHCII*$^{LSL/-}$, and *Xcr1*$^{Cre/+}$ *MHCII*$^{LSL/-}$ mice at steady state. **b**, (Left) Representative FACS analysis of splenic Treg percentage in *Xcr1*$^{+/+}$ *MHCII*$^{fl/fl}$ and *Xcr1*$^{Cre/+}$ *MHCII*$^{fl/fl}$ at steady state. (Right) Graph of splenic Treg percentage as a percentage of all CD4$^+$ T cells. Data are pooled biologically independent samples from two independent experiments ($n = 5$ for *Xcr1*$^{+/+}$ *MHCII*$^{fl/fl}$, $n = 4$ for *Xcr1*$^{Cre/+}$ *MHCII*$^{fl/fl}$). **c**, Representative FACs analysis and histograms of CFSE dilution of proliferated OT-II on day 3 after transfer into *Xcr1*$^{+/+}$ *MHCII*$^{fl/fl}$, *Xcr1*$^{Cre/+}$ *MHCII*$^{fl/fl}$, and *Xcr1*$^{Cre/+}$ *MHCII*$^{LSL/-}$ immunized with soluble OVA. **d**, Representative FACs analysis and histograms of CFSE dilution of proliferated OT-II on day 3 after transfer into *Xcr1*$^{+/+}$ *MHCII*$^{fl/fl}$, *Xcr1*$^{Cre/+}$ *MHCII*$^{fl/fl}$, and *Xcr1*$^{Cre/+}$ *MHCII*$^{LSL/-}$ immunized with cell-associated OVA.

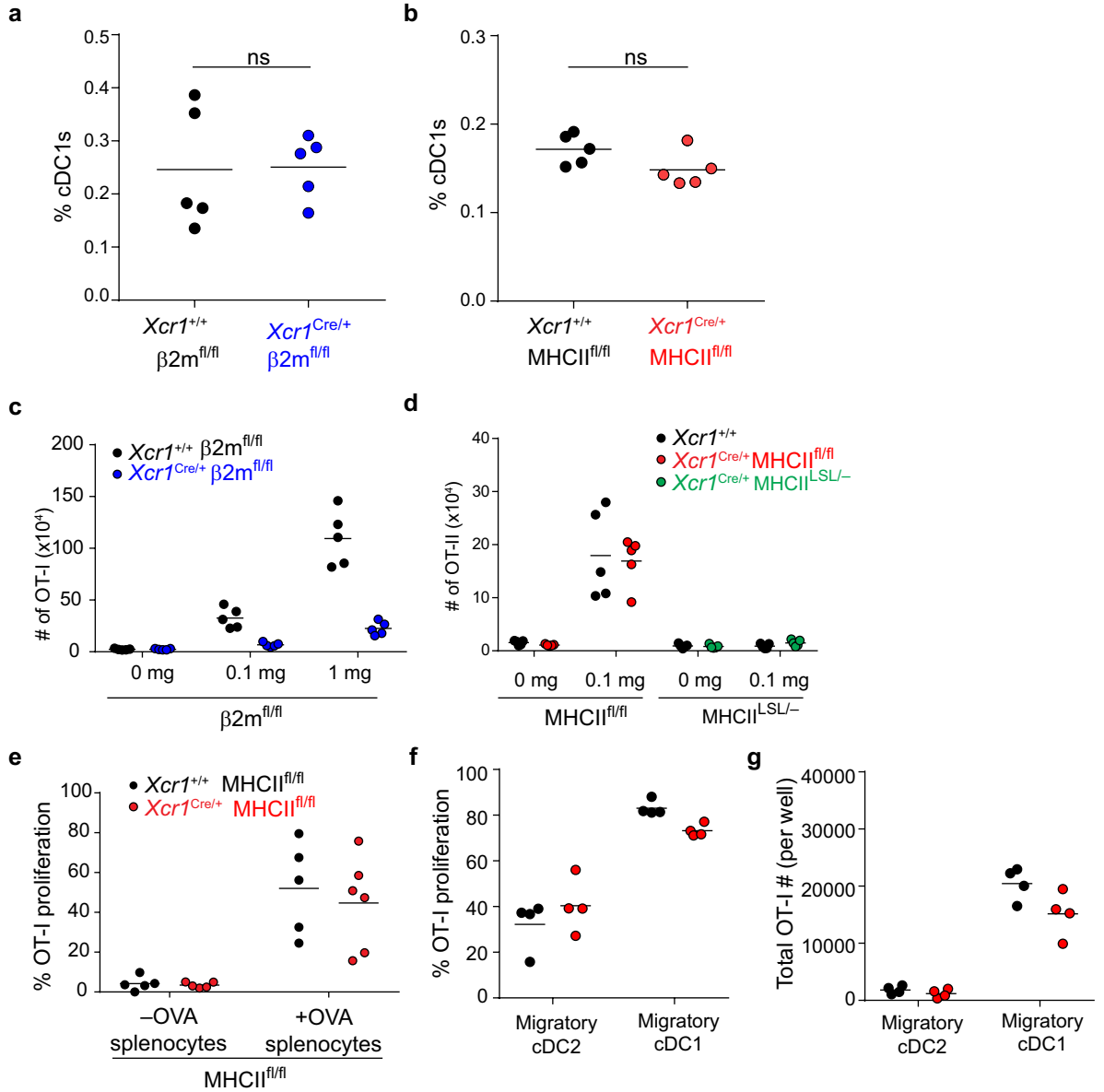

Extended Data Fig. 6 | Analysis of cDC1 in conditionally deleted mice. **a**, Graph of splenic cDC1 percentage in *Xcr1*$^{+/+}$ *β2m*$^{fl/fl}$ and *Xcr1*$^{Cre/+}$ *β2m*$^{fl/fl}$. Data are pooled biologically independent samples from two independent experiments ($n = 5$ for all groups). P = NS (unpaired, two-tailed Mann–Whitney test). **b**, Graph of splenic cDC1 percentage in *Xcr1*$^{+/+}$ *MHCII*$^{fl/fl}$ and *Xcr1*$^{Cre/+}$ *MHCII*$^{fl/fl}$. Data are pooled biologically independent samples from two independent experiments ($n = 5$ for all groups). P = NS (unpaired, two-tailed Mann–Whitney test). **c**, Graph of absolute numbers of transferred OT-I in soluble OVA treated *Xcr1*$^{+/+}$ *β2m*$^{fl/fl}$ and *Xcr1*$^{Cre/+}$ *β2m*$^{fl/fl}$ mice. Data are pooled biologically independent samples from two independent experiments ($n = 5$ for all groups). **d**, Graph of absolute numbers of transferred OT-II in soluble OVA treated *Xcr1*$^{+/+}$ *MHCII*$^{fl/fl}$ and *Xcr1*$^{Cre/+}$ *MHCII*$^{fl/fl}$ mice. Data are pooled biologically independent samples from two independent experiments ($n = 5$ for all groups). **e**, Graph of per cent proliferated OT-I in cell-associated treated *Xcr1*$^{+/+}$ *MHCII*$^{fl/fl}$ and *Xcr1*$^{Cre/+}$ *MHCII*$^{fl/fl}$ mice. Data are pooled biologically independent samples from two independent experiments ($n = 6$ for *Xcr1*$^{Cre/+}$ *MHCII*$^{fl/fl}$ OVA^{-} and OVA^{+} and $n = 5$ for all other groups). **f**, Graph of per cent proliferation of OT-I after 72 h coculture with ex vivo migratory cDC2 or cDC1 collected from tumour-draining lymph nodes of *Xcr1*$^{+/+}$ *MHCII*$^{fl/fl}$ or *Xcr1*$^{Cre/+}$ *MHCII*$^{fl/fl}$ mice injected 6 days earlier with 10^6 1956-mOVA cells. Cells were cultured at a ratio of 10:1 naive OT-I:cDC. Data are pooled independent samples from two independent experiments ($n = 4$ for all groups). **g**, Graph of absolute number of proliferated OT-I per well after 72 h coculture with ex vivo migratory cDC2 or cDC1 collected from tumour-draining lymph nodes of *Xcr1*$^{+/+}$ *MHCII*$^{fl/fl}$, *Xcr1*$^{Cre/+}$ *MHCII*$^{fl/fl}$ mice six days after injection with 10^6 1956-mOVA. Cells were cultured at 10:1 ratio of naive OT-I:cDC. Data are pooled independent samples from two independent experiments ($n = 4$ for all groups).

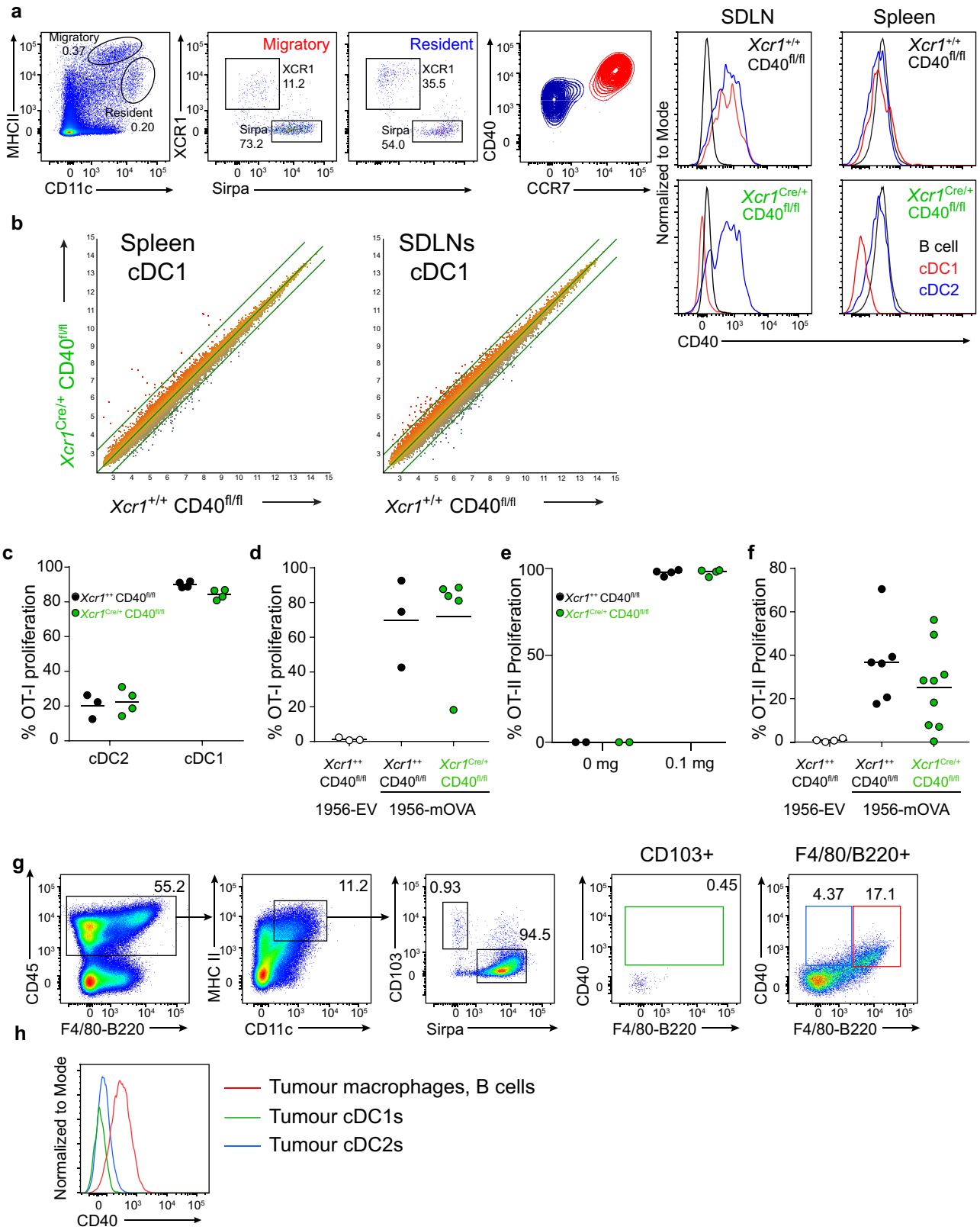

Extended Data Fig. 7 | See next page for caption.

Extended Data Fig. 7 | CD40 deficiency does not affect cDC1 development. **a**, SDLN flow cytometry gating for cDC1 expression of CD40. Migratory cDC1 (CD11c^{int} MHCII^{hi}; Red) were overlaid for expression with resident cDC1 (CD11c^{hi} MHCII^{int}; Blue). (Top) *Xcr1*$^{+/+}$ CD40$^{fl/fl}$ and (bottom) *Xcr1*$^{Cre/+}$ CD40$^{fl/fl}$ SDLN and splenic antigen-presenting cells stained for CD40 expression. **b**, Gene-expression data from *Xcr1*$^{+/+}$ CD40$^{fl/fl}$ and *Xcr1*$^{Cre/+}$ CD40$^{fl/fl}$ cDC1 from spleens and SDLN. Green lines indicate 2-fold changes. **c**, Graph of per cent proliferation of OT-I after 72 h coculture with ex vivo migratory cDC2 or cDC1 collected from tumour-draining lymph nodes of *Xcr1*$^{+/+}$ CD40$^{fl/fl}$ or *Xcr1*$^{Cre/+}$ CD40$^{fl/fl}$ mice injected 6 days earlier with 10^6 1956-mOVA cells. Cells were cultured at a ratio of 10:1 naive OT-I:cDC. Data are pooled independent samples from two independent experiments ($n = 3$ for *Xcr1*$^{+/+}$ CD40$^{fl/fl}$ cDC2 and $n = 4$ for all other groups). **d**, Graph of per cent proliferation of OT-I in tumour-draining lymph node of tumour-bearing mice 3 days after transfer. *Xcr1*$^{+/+}$ CD40$^{fl/fl}$ and *Xcr1*$^{Cre/+}$ CD40$^{fl/fl}$ mice were injected with 10^6 1956-EV or 10^6 1956-mOVA. Data are pooled independent samples from two independent experiments ($n = 5$ for *Xcr1*$^{Cre/+}$ CD40$^{fl/fl}$1956-mOVA, $n = 3$ for all other groups). **e**, Graph of per cent proliferation of transferred OT-II in soluble OVA treated *Xcr1*$^{+/+}$ CD40$^{fl/fl}$ and *Xcr1*$^{Cre/+}$ CD40$^{fl/fl}$ mice. Data are pooled biologically independent samples from two independent experiments ($n = 2$ for 0 mg *Xcr1*$^{+/+}$ CD40$^{fl/fl}$ and *Xcr1*$^{Cre/+}$ CD40$^{fl/fl}$ and $n = 4$ for all other groups). **f**, Graph of per cent proliferation of OT-II in tumour-draining lymph node of tumour-bearing mice 3 days after transfer. *Xcr1*$^{+/+}$ CD40$^{fl/fl}$ and *Xcr1*$^{Cre/+}$ CD40$^{fl/fl}$ mice were injected with 10^6 1956-EV or 10^6 1956-mOVA. Data are pooled biologically independent samples from three independent experiments ($n = 4$ for 1956-EV, $n = 6$ for 1956-mOVA *Xcr1*$^{+/+}$ CD40$^{fl/fl}$, and $n = 9$ for 1956-mOVA *Xcr1*$^{Cre/+}$ CD40$^{fl/fl}$). **g**, Gating strategy to delineate day 6 1956-mOVA tumour immune cell antigen-presenting cell populations. **h**, FACs histogram of CD40 expression on gated antigen-presenting cell populations from **e**.

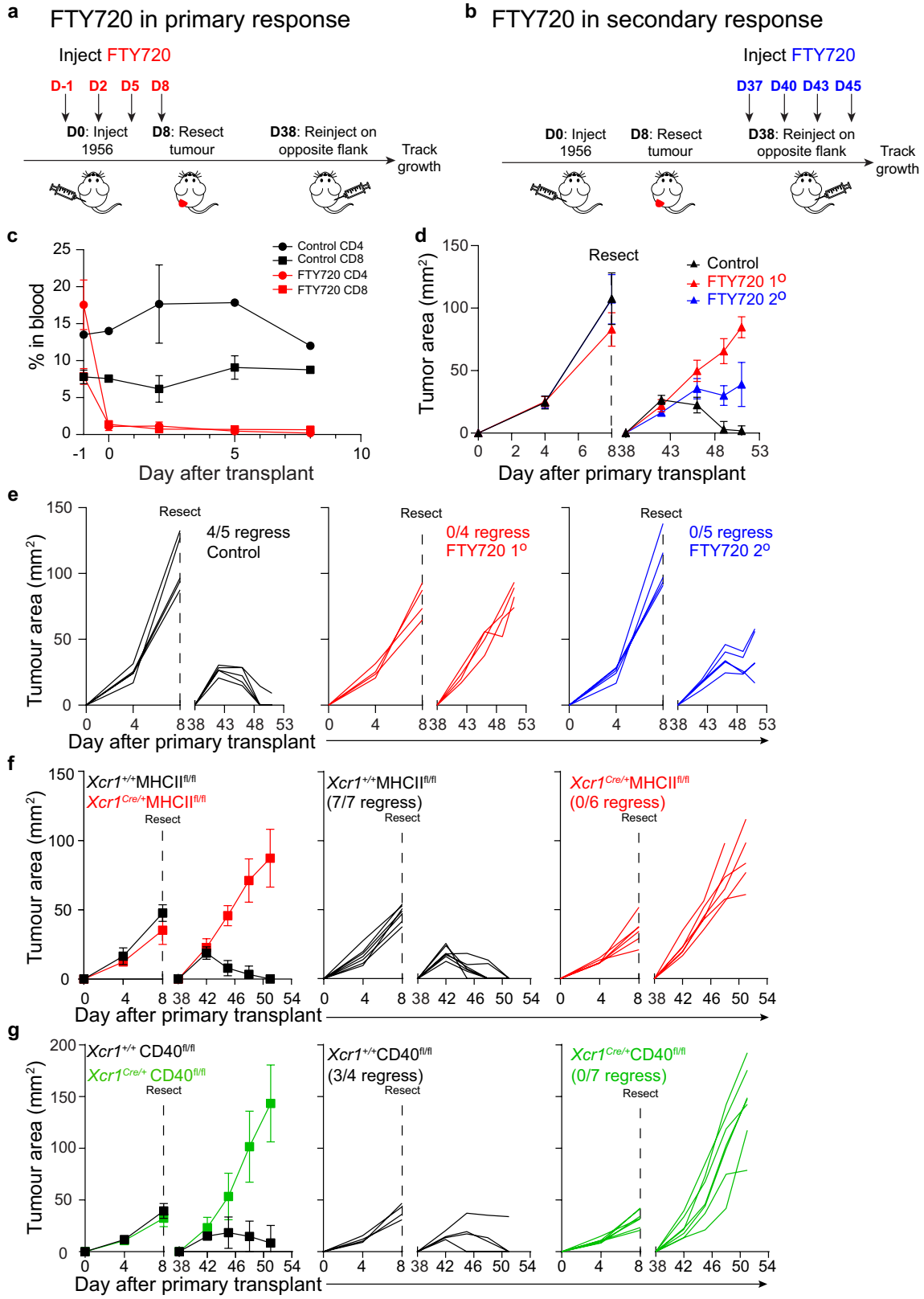

Extended Data Fig. 8 | See next page for caption.

Extended Data Fig. 8 | T cells are required at tumour site to induce memory. **a**, Schematic of FTY720 injection during primary tumour response. **b**, Schematic of FTY720 injection during secondary tumour response. **c**, Peripheral blood $CD4^+$ and $CD8^+$ T cell percentage in control and FTY720 treated mice. Data represent mean ± s.d. pooled biologically independent samples from two independent experiments ($n = 2$ control, $n = 5$ FTY720). **d**, Tumour growth curves of mice injected with FTY720 during the primary or secondary 1956 tumour implantation. Data represent mean ± s.d. pooled biologically independent samples from two independent experiments ($n = 4$ for FTY720 1° and $n = 5$ for all other groups). **e**, Individual mouse tumour growth curves of control or FTY720 injected mice. **f**, (Left) Tumour growth curves of *Xcr1*$^{+/+}$ *MHCII*$^{fl/fl}$ and *Xcr1*$^{Cre/+}$ *MHCII*$^{fl/fl}$ mice during primary and secondary 1956 tumour implantation. Individual mouse tumour growth curves of (middle) *Xcr1*$^{+/+}$ *MHCII*$^{fl/fl}$ or (right) *Xcr1*$^{Cre/+}$ *MHCII*$^{fl/fl}$ mice during primary and secondary 1956 tumour implantation. Data represent mean ± s.d. pooled biologically independent samples from two independent experiments ($n = 7$ for *Xcr1*$^{+/+}$ *MHCII*$^{fl/fl}$ and $n = 6$ for *Xcr1*$^{Cre/+}$ *MHCII*$^{fl/fl}$). **g**, (Left) Tumour growth curves of *Xcr1*$^{+/+}$ CD40$^{fl/fl}$ and *Xcr1*$^{Cre/+}$ CD40$^{fl/fl}$ mice during primary and secondary 1956 tumour implantation. Individual mouse tumour growth curves of (middle) *Xcr1*$^{+/+}$ CD40$^{fl/fl}$ or (right) *Xcr1*$^{Cre/+}$ CD40$^{fl/fl}$ mice during primary and secondary 1956 tumour implantation. Data represent mean ± s.d. pooled biologically independent samples from two independent experiments ($n = 4$ for *Xcr1*$^{+/+}$ CD40$^{fl/fl}$ and $n = 7$ for *Xcr1*$^{Cre/+}$ CD40$^{fl/fl}$).

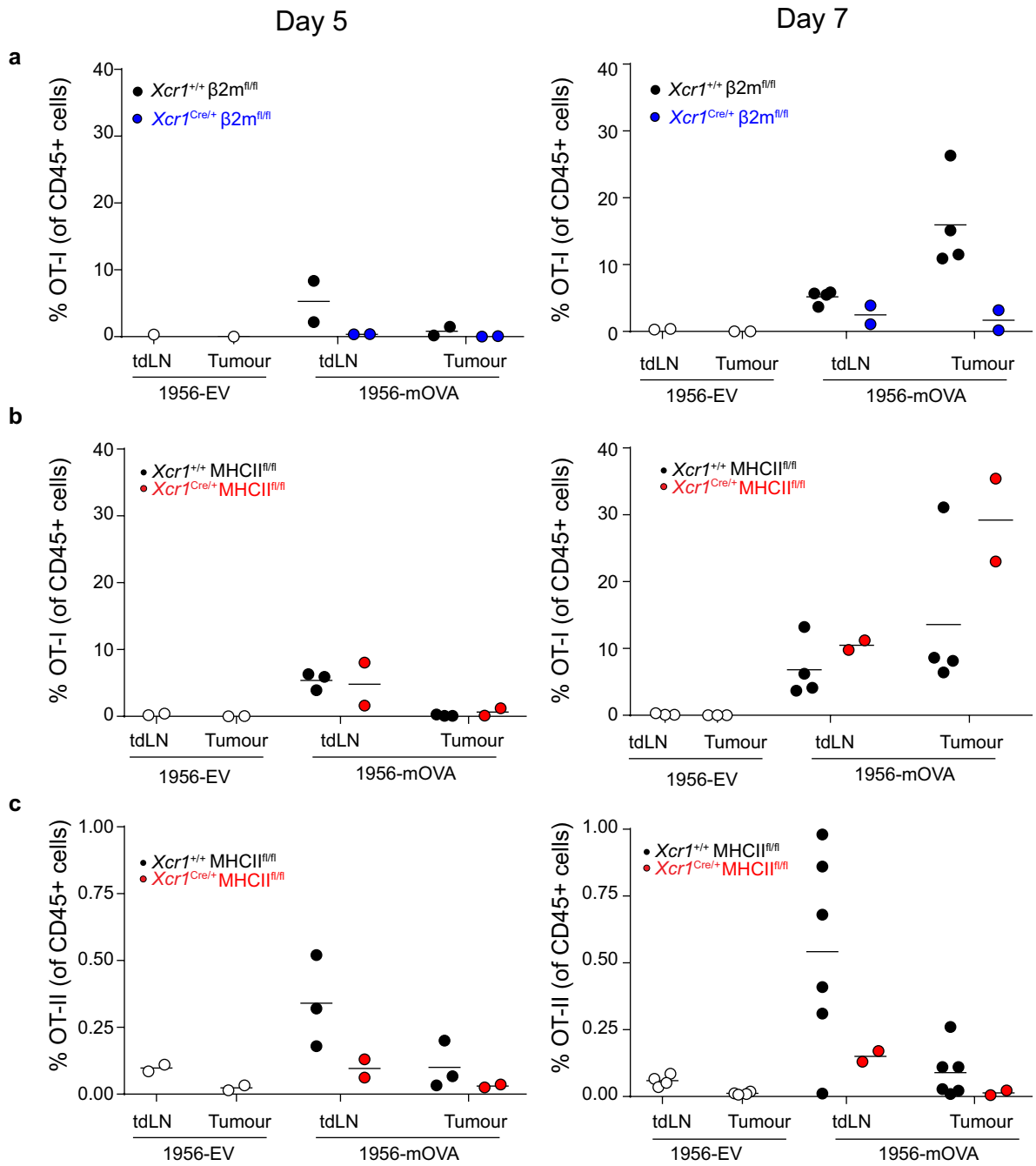

Extended Data Fig. 9 | OT-II CD4$^+$ T cells fail to localize to the tumour in *Xcr1*$^{Cre/+}$ *MHCII*$^{fl/fl}$ mice. a, Graph of per cent accumulation of transferred OT-I in tumours of *Xcr1*$^{+/+}$ *β2m*$^{fl/fl}$, *Xcr1*$^{Cre/+}$ *β2m*$^{fl/fl}$ injected with 10^6 1956-EV or 1956-mOVA on day 0. OT-I cells were transferred intravenously on day 2 and assessed as a percentage of total CD45$^+$ cells on (left) day 5 and (right) day 7. Data represent pooled biologically independent samples from two independent experiments ($n = 1$ for *Xcr1*$^{+/+}$ *β2m*$^{fl/fl}$ tdLN and tumour 1956-EV day 5, $n = 4$ for *Xcr1*$^{+/+}$ *β2m*$^{fl/fl}$ 1956-mOVA tdLN and tumour Day 7 $n = 2$ for all other groups). **b**, Graph of per cent accumulation of transferred OT-I in tumours of *Xcr1*$^{+/+}$ *MHCII*$^{fl/fl}$, *Xcr1*$^{Cre/+}$ *MHCII*$^{fl/fl}$ injected with 10^6 1956-EV or 1956-mOVA on day 0. OT-I cells were transferred intravenously on day 2 and assessed as a percentage of total CD45$^+$ cells on (left) day 5 and (right) day 7. Data represent pooled biologically independent samples from two independent experiments ($n = 4$ for *Xcr1*$^{+/+}$ *MHCII*$^{fl/fl}$ tdLN and tumour 1956-mOVA day 7, $n = 3$ for *Xcr1*$^{+/+}$ *MHCII*$^{fl/fl}$ tdLN and tumour 1956-mOVA day 5 and for *Xcr1*$^{+/+}$ *MHCII*$^{fl/fl}$ tdLN and tumour 1956-EV Day 7, $n = 2$ for all other samples). **c**, Graph of per cent accumulation of transferred OT-II in tumours of *Xcr1*$^{+/+}$ *MHCII*$^{fl/fl}$, *Xcr1*$^{Cre/+}$ *MHCII*$^{fl/fl}$ injected with 10^6 1956-EV or 1956-mOVA on day 0. OT-II cells were transferred intravenously on day 2 and assessed as a percentage of total CD45$^+$ cells on (left) day 5 and (right) day 7. Data represent pooled biologically independent samples from two independent experiments ($n = 6$ for *Xcr1*$^{+/+}$ *MHCII*$^{fl/fl}$ tdLN and tumour 1956-mOVA day 7, $n = 4$ for *Xcr1*$^{+/+}$ *MHCII*$^{fl/fl}$ tdLN and tumour 1956-EV Day 7, $n = 3$ for *Xcr1*$^{+/+}$ *MHCII*$^{fl/fl}$ tdLN and tumour 1956-mOVA day 5, $n = 2$ for all other samples).

nature research

Corresponding author(s): Kenneth M. Murphy

Last updated by author(s): Jun 12, 2020

Reporting Summary

Nature Research wishes to improve the reproducibility of the work that we publish. This form provides structure for consistency and transparency in reporting. For further information on Nature Research policies, see Authors & Referees and the Editorial Policy Checklist.

Statistics

For all statistical analyses, confirm that the following items are present in the figure legend, table legend, main text, or Methods section.

n/a	Confirmed	
☐	☒	The exact sample size (*n*) for each experimental group/condition, given as a discrete number and unit of measurement
☐	☒	A statement on whether measurements were taken from distinct samples or whether the same sample was measured repeatedly
☐	☒	The statistical test(s) used AND whether they are one- or two-sided *Only common tests should be described solely by name; describe more complex techniques in the Methods section.*
☒	☐	A description of all covariates tested
☐	☒	A description of any assumptions or corrections, such as tests of normality and adjustment for multiple comparisons
☐	☒	A full description of the statistical parameters including central tendency (e.g. means) or other basic estimates (e.g. regression coefficient) AND variation (e.g. standard deviation) or associated estimates of uncertainty (e.g. confidence intervals)
☐	☒	For null hypothesis testing, the test statistic (e.g. *F*, *t*, *r*) with confidence intervals, effect sizes, degrees of freedom and *P* value noted *Give P values as exact values whenever suitable.*
☒	☐	For Bayesian analysis, information on the choice of priors and Markov chain Monte Carlo settings
☒	☐	For hierarchical and complex designs, identification of the appropriate level for tests and full reporting of outcomes
☒	☐	Estimates of effect sizes (e.g. Cohen's *d*, Pearson's *r*), indicating how they were calculated

Our web collection on statistics for biologists contains articles on many of the points above.

Software and code

Policy information about availability of computer code

Data collection	Flow cytometry data was collected using BD FacsDiva software version 8.0
Data analysis	ArrayStar 14, FlowJO v.10, GraphPad Prism v.8

For manuscripts utilizing custom algorithms or software that are central to the research but not yet described in published literature, software must be made available to editors/reviewers. We strongly encourage code deposition in a community repository (e.g. GitHub). See the Nature Research guidelines for submitting code & software for further information.

Data

Policy information about availability of data

All manuscripts must include a data availability statement. This statement should provide the following information, where applicable:

- Accession codes, unique identifiers, or web links for publicly available datasets
- A list of figures that have associated raw data
- A description of any restrictions on data availability

The microarray data generated during the course of this study has been deposited and is available on the GEO database. The microarrays utilized in Figure 4b and Supplemental Extended data Figure 7b can be accessed with the following accession number: GSE152196. All other primary data and materials that support the findings of this study are available from the corresponding author upon request.

Field-specific reporting

Please select the one below that is the best fit for your research. If you are not sure, read the appropriate sections before making your selection.

☒ Life sciences ☐ Behavioural & social sciences ☐ Ecological, evolutionary & environmental sciences

For a reference copy of the document with all sections, see nature.com/documents/nr-reporting-summary-flat.pdf

Life sciences study design

All studies must disclose on these points even when the disclosure is negative.

Sample size	No formal power calculations were performed; however, the sample size of each group was robust and data was routinely collected across at least two independent replicates for each assay.
Data exclusions	No data was excluded from analyses
Replication	All experiments were replicated at least two different times with completely independent sets of mice that were the result of independent crosses. All replication attempts were successful.
Randomization	No formal randomization was performed as comparisons were done across mice of different genotypes, not across mice of the same genotypes receiving different treatments. No formal randomization was done across all other samples.
Blinding	Investigators were blinded to the genotype of the mice during sample preparation and data collection.

Reporting for specific materials, systems and methods

We require information from authors about some types of materials, experimental systems and methods used in many studies. Here, indicate whether each material, system or method listed is relevant to your study. If you are not sure if a list item applies to your research, read the appropriate section before selecting a response.

Materials & experimental systems

n/a	Involved in the study
☐	☒ Antibodies
☐	☒ Eukaryotic cell lines
☒	☐ Palaeontology
☐	☒ Animals and other organisms
☒	☐ Human research participants
☒	☐ Clinical data

Methods

n/a	Involved in the study
☒	☐ ChIP-seq
☐	☒ Flow cytometry
☒	☐ MRI-based neuroimaging

Antibodies

Antibodies used	Flow cytometry and cell sorting were completed on a FACS CantoII or FACS Aria Fusion instrument (BD) and analyzed using FlowJo analysis software (Tree Star). Staining was performed at 4ºC in the presence of Fc block (2.4G2) in magnetic-activated cell-sorting (MACS) buffer (PBS + .5% BSA + 2mM EDTA). The following antibodies were used; from BD Biosciences: CD117 (2B8), CD135 (A2F10.1), Ly6C (AL-21), MHCI (AF6-88.5), CD4 (RM4-5), CD8α (53-6.7), CD8β (53-5.8), CD11b (M1/70), B220 (RA3-6B2), CD64 (X54-5/7.1), CD19 (1D3), CD95 (Jo2), CD3 (145-2C11), CD45 (30-F11); from Tonbo Biosciences: MHCII (M5/114.15.2), CD44 (IM7), CD45.1 (A20), CD45.2 (104), CD11c (N418); from Biolegend: SA-BV605, SA-711, CCR7 (4B12), CD103 (2E7), XCR1 (ZET), CD115 (AFS98), Ter119 (Ter-119), Ly6G (1A8), TCRβ (H57-597), CD3 (145-2C11), CD8 (53-6.7), CD4 (RMA4-5), CD44 (IM7), CD40 (1C10), CD16/32 (93) ; from eBiosciences: TCRVα2 (B20.1), CD45.1 (A20), CD90.1 (HIS51), CD90.2 (53-2.1), F4/80 (BM8); from Invitrogen: CD172α (P84), CD45 (30F11); from Millipore/sigma: rabbit anti-ovalbumin (AB1225). For T cell depletions, 250 µg of depleting CD4 (YTS 191.1) or CD8 (YTS 169.4) antibodies (BioXcell) were injected intraperitoneallyv(IP) on day -4 and day 0 during the primary response or injected IP on day 34 and day 38 during the secondary response.
Validation	These antibodies have been validated by the manufacturer and by numerous citations as they are all antibodies in common use. Please see the manufacturer home pages for each antibody for the specific citations for each. All antibodies used for flow cytometry are commercially available and validation materials are available on the appropriate websites. Tetramers were validated by staining cell populations from tumors not expressing the indicated antigens.

Eukaryotic cell lines

Policy information about cell lines

Cell line source(s)	1956 source Schreiber lab, B16F10 source ATCC
Authentication	1956: Obtained from Dr. Robert Schreiber laboratory group, and not formally authenticated. B16F10: Obtained from ATCC, and not formally authenticated.
Mycoplasma contamination	Cell lines were tested and confirmed negative for Mycoplasma by Dr. Robert Schreiber laboratory group
Commonly misidentified lines (See ICLAC register)	There are no commonly misidentified lines in this study

Animals and other organisms

Policy information about studies involving animals; ARRIVE guidelines recommended for reporting animal research

Laboratory animals	Irf8 +32–/– were generated in house and described previously3035. IAβbstopf/f (MHCIILSL)3439 mice were provided by Gregory Wu (Washington University, St. Louis, MO). Mice harboring floxed alleles of β2-microglobulin (β2mfl)3237 were provided by Wayne Yokoyama (Washington University, St. Louis, MO). MHCI TKO mice (Kb–/–Db–/–β2m–/–) were originally provided by T. Hansen (Washington University, St. Louis, MO) 4751. C57BL/6J (B6), MHCIIfl (B6.129X1-H2-Ab1tm1Koni/J), C57BL/6-Tg(TcraTcrb)1100Mb/J (OT-I), C57BL/6- Tg(TcraTcrb)425Cbn/J (OT-II), B6.129X1-Gt(ROSA)26Sortm1(EYFP)Cos/J (R26LSLYFP), B6.SJL-Ptprca Pepcb/BoyJ (CD45.1) B6.129S4-Gt(ROSA)26Sortm1(FLP1)Dym/RainJ (R26FLP) were purchased from The Jackson Laboratory. CD45.1 mice were bred to OT-I and OT-II to produce CD45.1 OT-I and CD45.1 OT-II, respectively. The Cd40tm1a(KOMP)Wtsi mouse used for this project was generated by the trans-NIH Knock-Out Mouse Project (KOMP) and obtained from the KOMP Repository (www.komp.org). NIH grants to Velocigene at Regeneron Inc (U01HG004085) and the CSD Consortium (U01HG004080) funded the generation of gene-targeted ES cells for 8500 genes in the KOMP Program and archived and distributed by the KOMP Repository at UC Davis and CHORI (U42RR024244). The Cd40tm1a(KOMP)Wtsi trapping cassette "SA-βgeo-pA" (splice acceptor-beta-geo-polyA) flanked by Flp-recombinase target FRT sites was converted to a conditional allele by breeding to R26FLP mice. The resulting mice lack the gene trap cassette leaving two loxP sites flanking exons 2-4 of Cd40 (CD40fl). The resultant CD40fl mice were subsequently used in experiments where indicated. Xcr1Cre mice with germline deletion of MHCI, MHCII, or CD40 were excluded from our study. All in vivo experiments were performed in our specific-pathogen free facility and both sexes were used between the ages of 8 and 16 weeks. All animals were maintained on 12-hour light cycles and housed at 70ºF and 50% humidity. All experiments were performed in accordance with procedures approved by the AAALAC-accredited Animal Studies Committee of Washington University in St Louis and were in compliance with all relevant ethical regulations.
Wild animals	Study did not involve wild animals.
Field-collected samples	Study did not involve field-collected samples.
Ethics oversight	All mice were maintained in a specific pathogen–free animal facility following institutional guidelines and with protocols approved by the Animal Studies Committee at Washington University in St. Louis, an Institutional Animal Care and Use Committee (IACUC).

Note that full information on the approval of the study protocol must also be provided in the manuscript.

Flow Cytometry

Plots

Confirm that:

☐ The axis labels state the marker and fluorochrome used (e.g. CD4-FITC).

☒ The axis scales are clearly visible. Include numbers along axes only for bottom left plot of group (a 'group' is an analysis of identical markers).

☒ All plots are contour plots with outliers or pseudocolor plots.

☒ A numerical value for number of cells or percentage (with statistics) is provided.

Methodology

Sample preparation	Lymphoid and non-lymphoid organ DCs were harvested and prepared as described previously3035. Briefly, spleens and inguinal skin-draining LNs were minced and digested in 5ml of IMDM +10% FCS (cIMDM) with 250µg/ml of collagenase B (Roche) and 30 U/ml of DNaseI (Sigma-Aldrich) for 45min at 37°C with stirring. Lungs were minced and digested in 5ml of cIMDM with 4mg/ml of collagenase D (Roche) and 30U/ml of DNaseI (Sigma-Aldrich) for 1.5h at 37°C with stirring. TumorTumours were minced and digested in serum-free IMDM with 125µg/ml Liberase (Roche) and 30 U/mL of DNaseI (Sigma-Aldrich) for 45 minutes at 37°C with stirring. After digestion was complete, single-cell suspensions from all organs were passed through 70-µm strainers and red

	blood cells were lysed with ammonium chloride–potassium bicarbonate (ACK) lysis buffer. Cells were subsequently counted with a Vi-CELL analyzer (Beckman Coulter) and 3-5×106 cells were used per antibody staining reaction.
Instrument	BD FACSCanto II or BD FACSAria Fusion
Software	FlowJo V10
Cell population abundance	A FACSAria Fusion was used for sorting and cells were sorted into cIMDM. Sort purity of >95% was confirmed by post-sort analysis before cells were used for further experiments.
Gating strategy	Gating strategies for all cell populations are depicted within the paper. For FSC/SSC populations were gated as within the lymphocyte gate as has been traditionally done. Singlets were gated based on FSC-A/FSC-W profile as is traditionally done

☒ Tick this box to confirm that a figure exemplifying the gating strategy is provided in the Supplementary Information.